AD-A094 531 CINCINNATI UNIV OH DEPT OF MATERIALS SCIENCE AND MET--ETC F/G 7/4
SMALL-ANGLE X-RAY DIFFRACTION STUDY OF THERMAL TRANSITION IN ST--ETC(U)
JAN 81 R ROE, M FISHKIS, J C CHANG N00014-77-C-0326
UNCLASSIFIED TR-5 NL

1 OF 2
AD A 094531

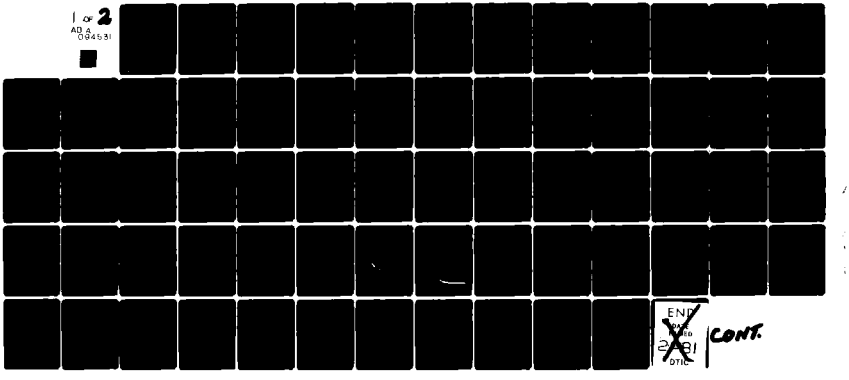

END
DATE FILMED
2-81
DTIC

CONT.

LEVEL

OFFICE OF NAVAL RESEARCH

Contract N00014-77-C-0376

Task No. NR 356-655

TECHNICAL REPORT NO. 5

Small-Angle X-Ray Diffraction Study of Thermal Transition in Styrene-Butadiene Block Copolymers

by

Ryong-Joon Roe, M. Fishkis

and J. C. Chang

Department of Materials Science and

Metallurgical Engineering

University of Cincinnati

Cincinnati, OH 45221

Prepared for Publication

in Macromolecules

January 15, 1981

SECURITY CLASSIFICATION OF THIS PAGE (When Data Entered)

(14) TR-5

REPORT DOCUMENTATION PAGE

READ INSTRUCTIONS BEFORE COMPLETING FORM

1. REPORT NUMBER: Technical Report No. 5	2. GOVT ACCESSION NO.: AD A094531
3. RECIPIENT'S CATALOG NUMBER: (1)	
4. TITLE (and Subtitle): (6) Small-Angle X-Ray Diffraction Study of Thermal Transition in Styrene-Butadiene Block Copolymers	5. TYPE OF REPORT & PERIOD COVERED: Technical Report
	6. PERFORMING ORG. REPORT NUMBER
7. AUTHOR(s): (10) Ryong-Joon Roe, M. Fishkis and J. C. Chang	8. CONTRACT OR GRANT NUMBER(s): (15) N00014-77-C-0326
9. PERFORMING ORGANIZATION NAME AND ADDRESS: Dept of Materials Science and Metallurgical Engineering, University of Cincinnati, Cincinnati, OH 45221	10. PROGRAM ELEMENT, PROJECT, TASK AREA & WORK UNIT NUMBERS: NR-356-655
11. CONTROLLING OFFICE NAME AND ADDRESS: (11) Office of Naval Research, Arlington, VA 22217	12. REPORT DATE: 15 Jan 1981
	13. NUMBER OF PAGES
14. MONITORING AGENCY NAME & ADDRESS (if different from Controlling Office): (12) 65	15. SECURITY CLASS. (of this report)
	15a. DECLASSIFICATION/DOWNGRADING SCHEDULE

16. DISTRIBUTION STATEMENT (of this Report)

Approved for Public Release; distribution unlimited

17. DISTRIBUTION STATEMENT (of the abstract entered in Block 20, if different from Report)

18. SUPPLEMENTARY NOTES

19. KEY WORDS (Continue on reverse side if necessary and identify by block number)

block copolymers, thermal transition, small-angle X-ray scattering, interface thickness

20. ABSTRACT (Continue on reverse side if necessary and identify by block number)

The small-angle X-ray scattering technique is utilized to study the transition in styrene-butadiene block copolymers from a microdomain structure to a disordered homogeneous phase. The transition, occurring on raising the temperature, is reproducible and thermally reversible. The SAXS intensity pattern, exhibiting a main interdomain peak and a few secondary peaks at room temperature, shows a gradual decrease in intensity over a temperature range of more than 100°, but the position and the

DD FORM 1 JAN 73 1473 EDITION OF 1 NOV 65 IS OBSOLETE

S/N 0102-LF-014-6601

405382

SECURITY CLASSIFICATION OF THIS PAGE (When Data Entered)

(continued from Block No. 20)

overall shape of the main peak remain unchanged. Analysis of the SAXS data shows that, with increasing temperature, the invariant and the length of inhomogeneity decrease, but the domain boundary thickness remains approximately constant. It is concluded that the disappearance of the microdomains proceeds by gradual intermixing of components into the opposite phases, with accompanying changes in the size of the microdomains, much in the same manner as would occur with coexisting phases of a binary liquid system. Even when the microdomains have finally disappeared and the mixture has become thermodynamically homogeneous, the SAXS pattern of diminished intensity persists, reflecting the presence of dynamic density inhomogeneity, as suggested in the theories by de Gennes and by Leibler. The similarity of our SAXS results with those obtainable with a supercooled mixture undergoing a spinodal decomposition is pointed out and its thermodynamic basis discussed.

ABSTRACT

The small-angle X-ray scattering technique is utilized to study the transition in styrene-butadiene block copolymers from a microdomain structure to a disordered homogeneous phase. The transition, occurring on raising the temperature, is reproducible and thermally reversible. The SAXS intensity pattern, exhibiting a main interdomain peak and a few secondary peaks at room temperature, shows a gradual decrease in intensity over a temperature range of more than 100°, but the position and the overall shape of the main peak remain unchanged. Analysis of the SAXS data shows that, with increasing temperature, the invariant and the length of inhomogeneity decrease, but the domain boundary thickness remains approximately constant. It is concluded that the disappearance of the microdomains proceeds by gradual intermixing of components into the opposite phases, with accompanying changes in the size of the microdomains, much in the same manner as would occur with coexisting phases of a binary liquid system. Even when the microdomains have finally disappeared and the mixture has become thermodynamically homogeneous, the SAXS pattern of diminished intensity persists, reflecting the presence of dynamic density inhomogeneity, as suggested in the theories by de Gennes and by Leibler. The similarity of our SAXS results with those obtainable with a supercooled mixture undergoing a spinodal decomposition is pointed out and its thermodynamic basis discussed.

I. INTRODUCTION

Interesting and unique properties of block copolymers arise from the fact that they often attain geometrically regular arrangements of microdomains consisting of components segregated from each other. Electron micrographs revealing beautiful arrays of spheres, cylinders and lamellae abound in the literature. The thermodynamic basis for such microdomain formation and the conditions leading to one or the other morphology have been enunciated by a number of workers[1-9] in the last decade.

On the basis of these theories and also of general thermodynamic considerations, one can expect that such microdomain structure becomes unstable under certain conditions and instead a homogeneous phase becomes a thermodynamically preferred one. Such a case will arise when the two components are very similar, when the block lengths are fairly short, when the temperature is raised or lowered (depending on whether the corresponding homopolymer pair exhibits a LCST or a UCST), or when a common solvent is added. It is of interest to know more about the characteristics of such a transition, for example the degree of abruptness of the change or the properties which exhibit discontinuity at the transition point. In practice such a transition may be encountered in some instances during processing of block copolymers at high temperatures. A transition phenomenon in general offers much more stringent tests of competing theories, because assumptions which may otherwise be approximately valid can become severely strained at the transition region.

Chang and Gale[10] and Gouinlock and Porter[11] studied rheological properties of a styrene-butadiene triblock copolymer sample and found a discontinuity in its dynamic viscosity within a fairly narrow temperature range, which was attributed to disappearence of microdomain structure. Williams and others[12] made light scattering studies on a number of styrene-butadiene block copolymers to

detect the transition on temperature change. The results were, however, somewhat inconclusive because of the experimental difficulty owing to the small size of the domains in comparison to the wave length of light. Ramos and Cohen[13] prepared block copolymers of isoprene and butadiene of fairly high molecular weights, which remained homogeneous down to their glass transition temperatures even though the corresponding homopolymer pair was not compatible. These are but a few of the examples reported in the literature which impinge upon the transition phenomena involving block copolymer systems.

Small angle X-ray scattering (SAXS) technique is utilized in this work for a systematic investigation of the thermally induced transition occurring in a diblock and triblock copolymer of styrene and butadiene. Both samples contain 25 percent styrene, and the triblock copolymer has a molecular size exactly twice that of the diblock copolymer. The triblock copolymer sample is the very same material with which the rheological studies mentioned above were performed. Earlier we made a detailed study of the phase separation behavior in binary polymer mixtures containing a polystyrene as the first component and a polybutadiene or a styrene-butadiene copolymer as the second, and from it the value of the polymer-polymer interaction parameter between the styrene and butadiene components was determined. Our present experimental results, taken together with the previously determined interaction parameter value, then offer a set of data against which theories dealing with the block copolymer stability can be tested quantitatively without using any adjustable parameters.

II. EXPERIMENTAL SECTION

A. Materials

The styrene-butadiene diblock copolymer is the sample designated B25/75 in the previous publication[14], and was kindly synthesized by Dr. H. L. Hsieh

of Phillips Petroleum Co. Its number- and weight-average molecular weights (by GPC) are 27,000 and 28,000, and contains 25 wt % styrene (and the molecular weight of the styrene block is therefore about 7,000). The microstructure of the butadiene component is 42% trans-1,4, 28% cis-1,4, and 30% vinyl unsaturation. The triblock copolymer is the experimental sample synthesized and distributed by Shell Chemical Co. under the designation TR-41-2445. The molecular weights of the styrene, butadiene and styrene blocks are 7,000, 43,000 and 7,000 respectively. The microstructure of the butadiene is 50% trans-1,4, 40% cis-1,4, and 10% vinyl. The electron-micrograph published in the literature[15] shows that this sample forms spherical microdomains of styrene at room temperature.

The two samples contain the same proportion of styrene. The size of the triblock copolymer is almost exactly twice that of the diblock copolymer. If two of the diblock copolymer molecules are joined at their butadiene ends, the resulting molecule will be identical to one of the triblock copolymer. Thus any difference observed between the two samples can be attributed to the effect of the number of blocks in a molecule.

B. Methods

SAXS measurements were performed with a Kratky camera, which was modified and fitted with a one-dimensional position-sensitive detector. Description of the modification made to the Kratky camera is published elsewhere[16]. The intensity data, collected in a multichannel analyzer, were transferred to a PDP 11/23 laboratory computer and the correction[16] for the non-uniformity of the detector efficiency along its window length was applied first before other usual corrections, such as for the background scattering, slit smearing, etc., were made. The intensity data were scaled to the absolute unit by comparison to the intensity obtained with a calibrated Lupolen sample[17] kindly furnished by Prof. O. Kratky.

The block copolymer sample, containing a small concentration of antioxidant,

was thoroughly degassed under vacuum to minimize the chance of bubble formation on subsequent heating, and was molded into a cavity in an aluminum sample holder, which was then sealed vacuum tight with thin Kapton H films (a product of E. I. duPont Co.) covered on both sides of the window. Cartridge heaters and a thermocouple inserted in the sample holder assembly were used, with a temperature controller, to regulate the temperature within about ± 1° up to 350°C.

III. RESULTS

A. Transition Temperature

Fig. 1 shows the small-angle X-ray scattering results obtained with the diblock copolymer at various temperatures. Here the slit-smeared intensity $\tilde{I}(s)$ is given against s, in a semi-log plot, where $s = 2\sin\theta/\lambda$, λ being the wave length. Similar results obtained with the triblock copolymer are shown in Fig. 2, this time on a linear scale for the intensity. The results for the two samples are very similar, and the different methods of plotting in Figs. 1 and 2 are to highlight the different aspects which each method emphasizes. Intensity curves obtained at some of the temperatures were omitted from Figs. 1 and 2 for the sake of clarity.

These scattering patterns are reproducible and thermally reversible, and therefore probably represent equilibrium properties of the samples. With the diblock copolymer the measurements at various temperatures were performed in the order: 20°, 100°, 75°, 20°, 140°, 125°, 20°, 200°, 20°, 170°, 20°, 50°, 20°, 225°, 246°, and 20°C. The scattering patterns at 20°C, determined several times, were indistinguishable from each other, except the last one obtained after the sample was heated to 246°C. With the scattering curves for the triblock copolymer shown in Fig. 2, the order of measurements were 20°, 200°, 140°, 20°, 170°, 20°, 200°, 20°, 100°, 20°, 200°, 250°, and 300°C. The same remark concerning the reproducibility and thermal reversibility apply here. To be mentioned,

however, is that in the case of Fig. 1 only a single diblock sample was used for all the data shown, while in the case of Fig. 2, a fresh sample of the triblock copolymer was used for the last three measurements at 200°, 250° and 300°C. The fresh sample was necessary because the first one, after experiencing the periods of high temperature, evidently became degraded and did not show a decrease in the scattering when subsequently heated to 250°C. The fresh sample heated directly to 200°C then showed the reduction in the peak intensity as expected.

The features revealed in Figs. 1 and 2 can be summarized as follows: (1) The intensity of scattering at angles smaller than about 0.006 $\mathring{A}^{-1}$ in s decreases with increasing temperature. (2) The shape and position of the peak, however, do not change with temperature. (3) The intensity of scattering at angles larger than 0.008 $\mathring{A}^{-1}$ increases with temperature. (4) As a result of the opposite trends in the low and high angle regions, the SAXS intensity curves obtained at different temperatures cross each other at about the same point near s = 0.007 $\mathring{A}^{-1}$. The interpretation of these observations will be taken up in detail later in the DISCUSSION section, but some brief remarks may be made here. The scattering in the small angle region around the main peak arises primarily from the microdomain structure present in these block copolymers. The decrease in the peak intensity, while maintaining its position and shape, suggests that the basic characteristics of the microdomain structure remain largely unaltered but the contrast between the domains and the surrounding matrix is gradually decreasing with temperature. The scattering at angles higher than the cross-over point arises mostly from thermal density fluctuation, which is inevitably present in every amorphous material, and its increase with temperature is expected.

In Fig. 3 the peak heights taken from the intensity curves in Figs. 1 and 2 are plotted against the temperature. The gradual disappearance of the main peak is

seen to occur over a temperature range from about 50° to 150°C for the diblock copolymer, and from about 100° to 250°C for the triblock copolymer. There is no indication of an inception of a sharp transition comparable for example to melting of semi-crystalline polymers.

B. Low Temperature Structure

Figs. 4 and 5 show the intensity I(s) corrected for the slit smearing effect. The data at 20°C are in electron unit (per unit volume of the sample), while the curves for successively higher temperatures are multiplied by a factor 0.1 to shift them vertically for clarity. In scattering curves at lower temperatures there exist, besides the main peak, some additional fine details which gradually deteriorate with temperature. They seem to disappear more or less completely beyond about 100°C for the diblock and about 170° for the triblock copolymer sample. We also note that the secondary peaks in the lower temperature curves of the diblock copolymer are much less prominant than the comparable peaks for the triblock copolymer sample, indicating that the microdomain structure in the former is less well developed even at room temperature.

Of the three peaks clearly recognizable in each of the curves at lower temperatures, the main peak at the lowest scattering angle (see Table I) is generally considered[18-21] to arise from the presence of a fairly well-defined distance between the nearest neighbor pairs of microdomains. The rather broad, smeared peak occurring at the highest scattering angle among the three is considered, on the other hand, to arise from intraparticle interference of X-rays scattered from a single spherical microdomain. The radius of the sphere is then given[27] by 0.92/s. The interdomain distance D and the radius a of the spherical domain thus evaluated are listed in Table I.

The second peak in each curve is located at a diffraction angle which is about 1.6 times the position of the respective main peak. Organization of the spherical

domains into a regular macrolattice, often revealed under electron-microscopic observations, is probably responsible for this secondary interparticle interference peak. If the lattice is simple cubic (with the unit cell dimension equal to D), (110) and (111) planes are expected to give rise to diffraction peaks at $\sqrt{2}$ and $\sqrt{3}$ times the main peak angle. If the lattice is body-centered cubic (with the unit cell dimension equal to $(2/3^{\frac{1}{2}})$ D), diffractions by (110) and (200) planes will show up at angles $(3/2)^{\frac{1}{2}}$ and $\sqrt{3}$ times the main peak angle. If the lattice is face-centered cubic (with the unit cell dimension equal to $\sqrt{2}$ D), diffractions by (111) and (200) planes will be present at $(3/2)^{\frac{1}{2}}$ and $\sqrt{2}$ times the main peak angle. For a given value of the inter-particle distance D, the density of lattice points differs somewhat among the three cubic lattice types. For the values of D and a listed in Table I, the volume fraction of the spherical domains calculated for the three lattice types are 16.7% (19.5%), 21.7% (25.3%) and 23.6% (27.6%) for sc, bcc, and fcc respectively (the values within the parentheses being those for the triblock sample). The sc lattice is ruled out because the calculated volume fraction is too far below 25%. The angular position of the observed secondary peak at 1.6 times the main peak angle agrees better with (200) plane of the bcc lattice than with (200) plane of the fcc lattice. The absence of an additional peak at $(3/2)^{\frac{1}{2}}$ times the main peak position, predicted for both bcc and fcc is, however, puzzling. In the literature both sc and fcc lattices were proposed for the observed diffraction patterns from block copolymer samples. This lack of agreement probably reflects some real differences among the samples studied, but may also come from a difficulty of assigning a unique lattice structure when in fact the lattice is not very regular.

C. High Temperature Structure

In both Figs. 4 and 5, the curves for the highest temperature still exhibit a small peak at about the same angle as the main peak obtained at other

temperatures. One can therefore wonder whether a remnant of the microdomain structure has persisted to the highest temperature we studied. de Gennes[22] earlier considered X-ray scattering from a liquid consisting of partially labeled polymer molecules, and numerical results of his theory applied to block copolymer systems were presented by Le Grand[23]. In Fig. 6, the desmeared intensity curve for the diblock copolymer at 200°C is compared with the curve calculated according to de Gennes' theory. (The numerical values of the physical parameters required for this calculation are: electron density difference between the components = 0.086 mole-electrons/cm^3, mol. wt. = 28,000, end-to-end distance = 142 Å, segment length = 2 Å. Different values for the segment length produce curves which are insignificantly different.) Both the observed and theoretical curves are given in electron units per unit volume. If we assume that there exists a contribution to the observed intensity by a component of scattering which rises steeply at very low angles, as illustrated by a broken curve in Fig. 6, then the size of the peak in the observed curve might be considered comparable to the one predicted by de Gennes' theory. Thus, it appears that the presence of a small peak in the high temperature curves indicates not a persistence of microdomain structure but rather the effect of the "correlation hole," or the fact that the two blocks belonging to the same molecule, even in a homogeneous phase, are contrained to maintain a fairly well-defined distance between them.

D. Thermal Density Fluctuation

In Fig. 7 the observed intensity $\tilde{I}(s)$ for the diblock copolymer sample is plotted against s^6. It is seen that at all temperatures the larger angle data lie roughly on a straight line, indicating the validity of approximating them by

$$\tilde{I}_b = a + b\, s^n \qquad (1)$$

with n = 6. Applicability of such an approximation, with n equal to some even number (4 or 6), was previously shown by others[20, 21, 24-26]. The data for the tri-

block copolymer, when plotted likewise, also follow eq. (1) fairly well. (Only the results for the diblock copolymer sample are presented explicitly here and in all the following when the features observed with the two samples are similar.)

When structural parameters based on a two phase model, such as the thickness of the phase boundaries, are to be evaluated, a correction has to be applied to the observed intensity $\tilde{I}(s)$ by subtracting from it the diffuse "background" represented by eq. (1). The power law approximation is also useful for obtaining the intensity $\tilde{I}(0)$ extrapolated to angle zero. The X-ray intensity scattered from a pure, single-component liquid - amorphous material consists solely of such "diffuse" background, and the zero-angle intensity is the measure[27-29] of the density fluctuation present in the liquid even under equilibrium condition. With our samples, the effect of the microdomain structure is reflected mostly in the lower angle region seen in Figs. 2, 4, and 5, and the diffuse scattering approximated by eq. (1) arises from the electron density fluctuations present within each microphases. In Fig. 8, I(0), the intensity (from the diblock copolymer) extrapolated to angle zero and corrected for the slit smearing, is plotted against temperature. Shown also for comparison is the extrapolated I(0) obtained with a polystyrene sample[30]. For a liquid in equilibrium, the zero angle intensity I(0) can be related to its thermodynamic properties by

$$I(0) = \rho^2 \, kT \, \beta_T \qquad (2)$$

where ρ is the mean electron density, β_T is the isothermal compressibility and I(0) is expressed in electron units per unit volume (i.e., electrons^2/cm^3). For polymers above T_g, observed intensity data[31,32] were shown to agree fairly well with eq. (2). Below T_g, the variation in I(0) with T is less[31-33] than predicted by eq. (2), and therefore in the plot of I(0) vs T a kink results at around

T_g, as is evident in the polystyrene data in Fig. 8. No comparable data for polybutadiene is available at present. Estimation of I(0) by means of eq. (2) can neither be made reliably because the value of β_T for PBD could not be found in the literature. The much larger thermal expansion coefficient of PBD suggests, however, that β_T for PBD should be larger than for PS. The electron density ρ for PBD is less than for PS on the other hand. As a result, I(0) for PBD may not be very different from the same for PS. When these considerations are taken together, the values of I(0) in Fig. 8 for the diblock copolymer appear to be in excess of the expected average of contributions from pure PS and PBD. A kink in the data for the diblock copolymer occurs at around 100°C and resembles the one in the PS data. The kink in the former is, however, unlikely to be the manifestation of a glass transition, since by differential scanning calorimetry, only a broad transition centered around 70~80°C could be recognized[34]. It could be that the "background" scattering, which is approximated by eq. (1), arises not only from thermal density fluctuation but also partly from concentration fluctuation within each microphase. This would be possible if the components dissolve gradually into each other as the temperature is raised. The fairly sudden change in the slope seen in Fig. 8 might then indicate an acceleration of this mutual dissolution with temperature.

E. Invariant

By integrating the observed intensity over the entire angular range, one can evaluate the invariant Q

$$Q = 4\pi \int_0^\infty s^2 I(s)\, ds. \qquad (3)$$

It is known that Q is equal to the mean square deviation $\langle (\delta\rho)^2 \rangle$ of the electron density from the mean throughout the sample. If, instead of the observed intensity,

the one from which the correction for the "background" is made is substituted for I(s) in the integrand of eq. (3), then the resultant Q represents only the contribution to the mean square electron density deviation by the coarse morphology in the sample, and excludes the contribution by the local heterogeneities due to thermal and concentration fluctuations. For data obtained with a camera approaching an infinite slit geometry, the slit-smeared intensity $\tilde{I}(s)$ can be integrated also to give

$$Q = 2\pi \int_0^\infty s\, \tilde{I}(s)\, ds \qquad (4)$$

In Fig. 9 the values of Q evaluated from eq. (4), with $\tilde{I}(s)$ corrected for the "background" according to eq. (1), are plotted against temperature. If the sample consists of only two types of domains divided by sharp boundaries, the mean square electron density deviation is given by

$$\langle (\delta\rho)^2 \rangle = (\rho_1 - \rho_2)^2 \; \phi_1 \, \phi_2 \qquad (5)$$

where ρ_1 and ρ_2 are the mean electron densities in each domain and ϕ_1 and ϕ_2 are the volume fractions. The solid curve in Fig. 9 is the one calculated by eq. (5) with $\phi_1 = 0.25$ and with ρ_1 and ρ_2 appropriate for pure PS and PBD at the corresponding temperatures. The kink in this curve arises from the glass transition of PS (taken as 80°C). At room temperature, the observed Q value is then only moderately below the ideal two phase value of eq. (5), indicating a fairly complete segregation of components into their respective microdomains. As the temperature is raised, the observed Q values fall below the ideal one. Such a decrease in Q may occur either because the components begin to dissolve into each other or because the domain boundaries become progressively more diffuse. More detailed discussion on these possibilities are given later in the DISCUSSION section.

It is surprising at first to find that the observed value of Q does not diminish toward zero as the temperature is raised. The result presented in Section IIIC indicates that the microdomain structure is totally destroyed, in the case of the diblock copolymer, by 200°C. Yet the value of Q above 200°C in Fig. 9 is still almost a third of the calculated ideal value. This is because, except at the lower temperatures studied, the two phase model no longer is a sufficiently good approximation to the structure present in our samples. In addition to the short-range electron density heterogeniety represented by the "background" and the relatively long-range heterogeneity associated with the microdomain structure, there now arises an increasingly important contribution by an intermediate-range heterogeneity. The latter effect can be seen in Fig. 7, where the departure of the intensity from the more-or-less horizontal "background" is shown to persist to higher angles as the temperature is increased.

F. Interface Thickness

The SAXS technique is at present probably the only method capable of giving information on the thickness of microdomain interfaces. The principle of its method, first proposed by Ruland[35], has been elaborated since then by many workers[20,21,25,26,36-38]. The intensity I(s) (after correction for slit-smearing, if any), scattered from a sample consisting of two-phase structure, can be written as

$$I(s) \sim \frac{1}{8\pi^3} S (\rho_1 - \rho_2)^2 s^{-4} e^{-4\pi^2\sigma^2 s^2} + I_b \qquad (6)$$

for the scattering angle s in the Porod's region, where the intensity due to the two-phase structure decays toward zero. In eq. (6) S is the total surface area of the phase boundaries, σ is the measure of the diffuseness of the boundary

layer and I_b is the "background," which in this work is approximated by eq. (1). Eq. (6) is exact when the density profile across the interface can be represented by a convolution product of a step function and a gaussian smoothing function having σ^2 as its variance. An expression, equivalent to eq. (6) but applicable exactly to the density profile satisfying thermodynamic equilibrium conditions, is derived in Appendix. If the reciprocal of the density gradient at the center of the interface is taken as the effective thickness t, its relation to σ is dependent on the shape of the density profile, and is given by

$$t_{gauss} = \sqrt{12}\,\sigma \qquad \text{(gaussian profile)} \qquad (7a)$$

$$t_{eq.} = (4\sqrt{3}/\pi)\,\sigma \qquad \text{(equilibrium profile)} \qquad (7b)$$

Utilization of eq. (6) for determination of σ requires the solution of several practical problems. (1) The background I_b has to be evaluated reliably and subtracted from the observed intensity. (2) The observed intensity has to be either corrected for the slit-smearing effect or alternatively an equivalent method applicable directly to slit-smeared intensity has to be devised. (3) Criteria have to be established for recognition of the scattering angle at which the Porod's region indeed begins to a given degree of approximation. (4) The effect of the propagation of the statistical errors present in the observed intensity to the evaluated values of σ has to be assessed. The above four, somewhat interrelated, problems are all important because the effect to the observed intensity associated with each of these problems are often much larger individually than the effect of the diffuseness of the boundary represented by the factor $\exp(-4\pi^2\sigma^2s^2)$ in eq. (6).

We investigated three different methods of evaluating σ. When eq. (6) is linearized by expanding the exponential and retaining only the first two terms, one can easily perform the integration representing the slit-smearing effect, and obtains the following equation applicable to infinite slit geometry:

$$\tilde{I}(s) \sim \text{Const } s^{-3} (1 - 8\pi^2\sigma^2 s^2) + \tilde{I}_b \quad . \qquad (8)$$

Such an approximation is of course valid only for s smaller than $1/\sigma$. This equation allows easy graphical evaluation of σ by plotting either $\tilde{I}(s)\, s^3$ against s^2 or $\tilde{I}(s)s$ against s^{-2}. These alternative methods of plotting place respectively heavier weighting to data points at different angular regions. Fig. 10 shows the results for the diblock copolymer sample at 20°, 100° and 200°C, plotted according to the second way of plotting. From the slope and the intercept σ values are calculated to be 3.83Å, 3.71Å and 3.45Å respectively. Plots of $\tilde{I}(s)s^3$ vs s^2 give virtually identical values 3.85Å, 3.71Å and 3.42Å. In these plots the background scattering $\tilde{I}_b$ was subtracted by use of eq. (1) with the constants a and b evaluated from Fig. 7. It is surprising that the σ value does not change appreciably even as the temperature is raised to 200°C, at which the microdomain structure no longer remains. Although the ratio of the intercept to the slope decreases only moderately, the slope itself is reduced considerably at higher temperature, and also the angular range of straight line fit is reduced. For the angular range in Fig. 10 in which straight line fit appears valid, $2\pi\sigma s$ is between about 0.6 and 0.9, which makes the linearization of $\exp(-4\pi^2\sigma^2 s^2)$ a very poor approximation. In such cases the value of σ is known[37] to be underestimated.

Recently Koberstein, Morra and Stein[37] proposed a method by which the error in σ arising from linearization of eq. (6) can be avoided. They find that, when

eq. (6) is obeyed, the intensity $\tilde{I}(s)$ obtained with an infinite slit geometry can be represented to an excellent approximation, up to a much larger value of s, by

$$\tilde{I}(s) \sim K' \; s^{-3} \exp\left[-38(\sigma s)^{1.81}\right] \qquad (9)$$

where 38 and 1.81 are empirically determined constants. One may then plot $\ln[\tilde{I}(s)\, s^3]$ vs. $s^{1.81}$ to evaluate σ as $(-\text{slope}/38)^{1/1.81}$ or plot $s^{-1.81} \ln[\tilde{I}(s)\, s^3]$ vs $s^{-1.81}$ to evaluate σ as $(-\text{intercept}/38)^{1/1.81}$. Fig. 11 shows the data for the diblock copolymer at 20°, 100° and 200° according to the second scheme of plotting. The σ values calculated from the intercepts are 6.4, 5.7 and 5.0Å respectively and, as expected, are much larger than the values obtained from eq. (8).

In the third approach to the evaluation of σ, we employed a numerical, rather than graphical, method of analysis. Its starting point is

$$\tilde{I}(s) = C_1 F_1(s) + C_2 F_2(s) + C_3 s^n + C_4 \qquad (10)$$

where $F_1(s)$ and $F_2(s)$ are functions which depend on the slit geometry[36] and approach s^{-3} and s^{-1} respectively when the slit length becomes infinite. The last two terms embody $\tilde{I}_b$ as given by eq. (1). Eq. (10) is thus essentially the same as eq. (8). A computer program then performs a least squares evaluation of the four unknown constants C_1 - C_4 and their variances, when the value of n (either 4 or 6) and the angular range of the data to be included are specified. σ is then obtained as $(-C_2/C_1)^{1/2}/2\pi$. For a given set of data the program is run repeatedly with different angular ranges over which the least squares method is to be applied. A meaningful result, containing a negative value of C_2, is obtained only when an appropriate angular range is specified. Even when the solution for σ is attained, its value

varies widely for different angular ranges specified. The best fitting value of σ is decided on two criteria: the smallest variance of σ and the smallest root-mean-square deviation of $\tilde{I}(s)$ calculated by eq. (10) from the observed one. Table 2 summarizes the results obtained by the least squares method for selected temperatures. The error limits quoted are the standard deviation. The values of C_4 obtained by the numerical method agree with those evaluated graphically from Fig. 7 fairly well (within 5% in most cases). The angular range of data which was specified for the least squares analysis is also indicated. When the angular range specified is altered, the evaluated value of σ often changes much more than the standard deviation indicated in the Table suggests. Thus, when the uncertainty in the proper angular range to be included in the least square analysis is taken into account, the overall error is much larger than is given in Table II.

Summarizing the results obtained by the three different methods of evaluating the interface thickness parameter σ, it can be said that its value probably lies between 4 and 7 $\mathring{A}$ and does not change appreciably with temperature, (or if anything, it may decrease somewhat at higher temperature).

G. Porod's Length of Inhomogeneity

For a two-phase material a measure of the size of the domains can be given by the quantity l_p, known as Porod's length of inhomogeneity, which is related to the average chord lengths $\langle l_1 \rangle$ and $\langle l_2 \rangle$ of phases 1 and 2 by

$$1/l_p = 1/\langle l_1 \rangle + 1/\langle l_2 \rangle. \qquad (11)$$

It is also related to the specific interface area S/V between the phases by

$$1/l_p = (S/V)/(4\phi_1\phi_s). \qquad (12)$$

The intensity in the Porod's region can be written, by substituting (12) into (6), as

$$I(s) \sim \frac{V\phi_1\phi_2 (\Delta\rho)^2}{2\pi^3 l_p} s^{-4} e^{-4\pi^2\sigma^2 s^2} + I_b \qquad (13)$$

For a material in which the boundary between the microphases has a finite thickness t, the invariant Q is given (see Appendix) by

$$Q=V(\Delta\rho)^2 \phi_1\phi_2 (1 - t/l_p) \qquad (14)$$

and therefore (13) becomes

$$I(s) \sim \frac{Q}{2\pi^3(l_p - t)} s^{-4} e^{-4\pi^2\sigma^2 s^2} + I_b \qquad (15)$$

The constant C_1 in eq. (10), which is determined in the process of evaluating σ, is equal to $Q/2\pi^3 (l_p - t)$. The values of l_p obtained by

$$l_p = Q/(2\pi^3 C_1) - (4\sqrt{3}/\pi)\sigma \qquad (16)$$

are listed in Table II. A trend of l_p decreasing with temperature is clearly recognizable.

IV. DISCUSSION

The SAXS data collected in this work show clearly that the microdomain structure present at room temperature disappears gradually as the temperature is raised. At room temperature the segregation of styrene and butadiene components is probably fairly complete. The following evidence can be cited toward this conclusion. a) The SAXS pattern at low scattering angle can be interpreted in terms of

spherical microdomains placed on a cubic lattice. The intensity pattern is very similar to those obtained by others[18-21] with di- and triblock copolymers (either styrene-butadiene or styrene-isoprene) of much higher molecular weights. The inter- and intra-domain interference peaks observed here are somewhat less well defined, indicating that the shape and the ordering of the microdomains are less regular because of the lower molecular weights of our samples. b) The values of the invariant Q determined experimentally at room temperature are only slightly below the value calculated for an ideal two phase system with complete segregation of components and sharp boundaries. c) The triblock copolymer sample was examined by electron-microscopy by Chung et al[15] and was found to have spherical domains when the sample was prepared at room temperature. The staining, necessary for electron microscopy, is itself a chemical reaction modifying the nature of the polymer (likely to enhance any tendency possessed inherently for microphase separation), and therefore its detection in stained samples is not necessarily a proof of domain structure in the original unstained material, but it certainly reinforces the evidence obtained by other techniques. d) By differential scanning calorimetry, both of our samples were found[34] to have a very broad glass transition temperature around 70~80°C, suggesting that domains consisting mostly of polystyrene exist at room temperature.

Destruction of the microdomain structure at the higher end of the temperature range we studied appears to be also fairly complete. The SAXS peak at lower angular region is all but vanished. The residual peak which persists to high temperature lacks details attributable to inter- or intra-domain interference. Both the shape and the absolute magnitude of the residual peak compares favorably with the prediction by de Gennes[22] for a randomly mixed block copolymer system.

The question that remains is then on the structures in the intermediate temperatures which the material adopts in the gradual transition from one consisting of

segregated microdomains to a random mixture. A number of possible intermediate structures can be conceived but in Fig. 12 we depict two models which might be considered representative of two extreme ends of the possible spectrum. In Model I, the domain boundaries become more diffuse, while the effective size and the density at the centers of the domains remain unaltered. In Model II, the thickness of the domain boundaries is preserved but the compositions of the two microphases approach each other by intermixing of components. In this case the domain size may also change if the mutual dissolution into the opposite domains is unbalanced.

The interface thickness, determined by examination of the deviation from Porod's law, shows no sign of increasing with temperature and Model I therefore would have to be ruled out immediately on this account. A question might be raised about the reliability of the interface thickness so determined in view of the fact that the method still yields a finite interface thickness at high temperatures when a two phase structure no longer survives. This contradiction, however, arises mainly because Porod's law and its associated results, applicable only on two phase systems, are applied on structures which cannot be considered a two-phase system even in a very approximate sense. The thickness values obtained are likely to be meaningful only as long as the microdomain structure is still there. The results indicating no change in the thickness at low to intermediate temperature should, however, be considered valid, and weigh heavily against Model I.

The observed values of Q, presented in Section III E, fall progressively at higher temperatures below the calculated values expected of an ideal two-phase structure. Such a decrease in Q can be explained in terms of Model II, in which the electron density contrast between the two types of domains gradually diminish. Let us, however, examine whether the same decrease in Q might not be consistent with Model I also. In Appendix, the relative decrease y in Q is shown to be related to the interface thickness t by

$$y = t/l_p \qquad (17)$$

where y is $1-Q/Q_0$, Q_0 being the value expected of an ideal two phase system having sharp boundaries. When a spherical particles of radius a are imbedded in a continuous matrix, l_p is given by

$$l_p = \frac{4}{3} a(1-\phi_1) \qquad (18)$$

ϕ_1 being the volume fraction of the spheres. In Model I ϕ_1 remains equal to the initial value 0.25 at all temperatures, and l_p is then equal to the radius a. Fig. 9 shows that the experimental Q values are observed to fall to about 1/3 of the calculated ideal value, and thus would be realized, in terms of Model I, if the interface thickness becomes to about 2/3 of the radius, or about 50Å (radius a being equal to about 70°Å, see Table I). Thus the decrease in the observed Q value, by itself, might be reconciled with Model I, but of course the required thick interface disagrees with the value of σ evaluated from the intensity in the Porod's region.

We may note here that, despite the expectation that the microdomain structure vanishes at high temperature, the observed Q value is not reduced to zero. This, however, is no contradiction, since even without a two-phase structure there still exists local inhomogeneities in electron density due to concentration fluctuation which contributes to the experimentally determined Q value.

More direct discrimination between Models I and II can be attained by examination of the SAXS intensity pattern directly. The following qualitative, very approximate assessment may first be made in favor of Model II. The intensity I(s) is a Fourier transform of the correlation of distances in the real space. According to Model I, the correlation of the distance corresponding to the separation between the microdomains should not suffer any decrease with temperature, while the short range correlation, corresponding to distances within the microdomains, should greatly diminish at higher temperatures. Model I therefore predicts constancy of intensity at low angle but a rapid decrease in intensity at larger s

with the temperature. This is contrary to the experimental observation. Model II on the other hand predicts a decrease in I(s) at low s as well as at high s with increasing temperature. This is more in agreement with the experiment.

To put the above argument on a more quantitative basis, we make the following simple calculation. When a sample consists of identical particles imbedded regularly in a continuous matrix, the intensity can be written as

$$I(s) = f(s) \cdot g(s) \tag{19}$$

where the shape function f(s) depends only on the shape of the particle and the lattice function g(s) only on the arrangement of the particles on the lattice. When the lattice is very regular g(s) is of course sharply localized to various orders of Bragg angles. When the particles differ from each other somewhat in their shape and size, eq. (19) may still be approximately valid when an average form factor is used for f(s). We now calculate the form factor f(s) appropriate to either Model I or Model II. For Model I it can be written as

$$f_1(s) = \int (\Delta\rho_0)^2 \, \phi^2(s,a) \, H^2(s,t) \, w(a) \, da \tag{20}$$

where $\Delta\rho_0$ is the electron density difference $\rho_1 - \rho_2$ between the phases, $\phi^2(s,a)$ is the form factor for a sphere of radius a, $H^2(s,t)$ is the correction due to a diffuse interface of thickness t and w(a) is a distribution of sphere radius a. The scattering from a sphere is given[27] by

$$\phi(s,a) = (4/3) \, \pi \, a^3 \, U(2\pi sa) \tag{21}$$

with

$$U(x) = 3(\sin x - x \cos x)/x^3. \tag{22}$$

An expression for $H^2(s,t)$, applicable to the interface density profile determined by equilibrium condition, is given in Appendix. The distribution w(a) of sphere radius is assumed here in order to moderate the sharp valleys present in the sphere scattering function $\phi(s,a)$. Following Fujimura et al[21] we take a gaussian

function

$$w(a) = (2\pi\sigma_a^2)^{-\frac{1}{2}} \exp\,[-(a-\bar{a})^2/2\sigma_a^2] \qquad (23)$$

with σ_a equal to 0.2 $\bar{a}$. In Fig. 13 $f_1(s)$ is plotted against s for $\bar{a}$ = 70Å and t = 14Å in curve 1 and t = 42Å in curve 2. For ϕ_1 = 0.25, these t values correspond to the decrease in Q by 20 and 60% below the ideal value, respectively.

For Model II $f_2(s)$ would be similar to $f_1(s)$ in eq. (20) but now $(\Delta\rho_0)^2$ has to be replaced by $(\Delta\rho)^2$ reflecting the reduced electron density contrast between the phases, and the average radius $\bar{a}$ is also altered, but t would be kept constant at 14Å. $\Delta\rho$ and $\bar{a}$ are related to each other by the condition of conservation of mass. For curve 3 the values of $\Delta\rho = 0.875\ \Delta\rho_0$ and $\bar{a}$ = 58.09Å are used. These are the values which would be realized if Q is reduced to $0.40Q_0$ as some of the styrene segments dissolved into the butadiene domains but not vice versa.

Comparison of curves 1 and 2 shows that the increase in the interface thickness is reflected mainly in the large drop in the intensity at large s, without affecting it in the region of s smaller than about 0.01Å^{-1}. The experimental data show that the lattice factor g(s), due to the cubic arrangement of the spheres, has the main peak at s ~ 0.005Å^{-1}. Around this value of s, Model I would therefore predict the intensity to be about the same irrespective of temperature. On the other hand, curve 3 shows that the effect of the reduced electron density contrast is to reduce the intensity at all angles, but the effect is more pronounced at low angles where the main peak of g(s) is located. Both the qualitative argument presented earlier and the calculation based on the simple model demonstrate that the experimental data is more consistent with the view that gradual intermixing of the two components rather than broadening of the interface region is what results when the temperature is raised.

On the basis of the above analysis and of various evidence obtained in this work we propose the following morphological change as taking place on increasing

the temperature. At room temperature segregation of the componenets into domains is fairly complete, the styrene segments being confined in the spheres of radius 70Å and interface thickness 10 ~ 20Å. A degree of irregularity in the shape and size of the styrene domains and in their lattice-like arrangement exists already at room temperature even under equilibrium conditions. As the temperature is raised, intermixing of components between the spherical domains and the surrounding matrix increases. Because of the larger sequence length of the butadiene block and the smaller size of the spherical domains, the dissolution of butadiene segments into the latter occurs to a much smaller extent than the dissolution of styrene segments into the continuous matrix. As a result, the size of the spherical domains decreases, but its composition remains a nearly pure styrene. While the spheres become smaller, their number, the average distance between neighbors, and the thickness of the interface all remain mostly unaltered, but the regularity of the lattice and of the shape may deteriorate further.

We can envisage a sort of "phase-diagram", relating the composition of the spherical and matrix phases as a function of temperature, as depicted with heavy lines in Fig. 14. At point A there, the concentration of styrene in the continuous matrix becomes 25%, and the size of the spherical domains (of concentration still very high in styrene) reduces to zero. Above temperature T_A, the material is thermodynamically homogeneous and consists of a true single phase. The "phase" diagram in Fig. 14 of course resembles the phase diagram of a binary liquid mixture, but the portion above T_A, drawn light, is never realized. Although the material is homogeneous at temperatures above T_A, the SAXS intensity does not vanish at T_A. Dynamic density fluctuations produced from clustering of like components in homogeneous mixtures still produce measurable X-ray and light scattering as shown by Leibler[9], Scholte[39] and others[40]. For our diblock copolymer sample, T_A is believed to be between 100 and 150°C. Above T_A, as the degree of clustering

decreases with increasing temperature, the SAXS intensity also diminishes, until at sufficiently high temperature the only density inhomogeneity (other than that due to thermal density fluctuation) is the one dictated by the styrene and butadiene segments being bound to each other's proximity by covalent bonds. Below T_A, the SAXS intensity is contributed by the permanent domain structure as well as by the dynamic density fluctuation present within each phase. As the temperature is lowered much further below T_A, the contribution by the permanent domains of course predominates.

The evidence for the decrease in the size of the spheres with temperature comes from the data on Porod's length of inhomogeneity l_p shown in Table II. For a structure having spherical particles in a continuous matrix, eq. (18) holds. Since the factor $1-\phi_1$, initially equal to 0.75, can increase at most to 1, any decrease in l_p has to come from a reduction in the radius a. The value of l_p given in Table II does not diminish to zero even at the highest temperature. This contradicts the view schematically represented by Fig. 14, according to which no spherical domains remain about T_A. This apparent contradiction arises because eq. (13), used for the evaluation of l_p, is valid only as long as the electron density inhomogeneity is due solely to a two-phase structure. Thus, the values of both l_p and t, evaluated by the methods based on a two-phase structure, become erroneous at temperatures near and above T_A.

No theories of block copolymer systems available at present predict the gradual intermixing of two components as envisaged above. Most of the early theories[1-8] deal with the micro-domain structure obtained at temperatures far below the transition temperature, and will probably require modification to apply to the transition phenomenon. The recent theory by Leibler[9] explicitly addresses itself to the problem of thermally induced transition, and merits comparison here with our experimental findings. The theory predicts that, immediately below a well-defined transition temperature, the material adopts an ordered structure with spherical microdomains on bcc lattice, while above the transition

the spherical domains give way to a thermodynamically homogeneous, disordered phase. The SAXS pattern exhibited by the material below the transition would consist of sharp diffraction peaks, while the disordered phase will continue to give a SAXS pattern consisting of a single broad maximum, with the intensity gradually decreasing with temperature. In the limit of high temperature, the prediction of Leibler's theory approaches that of de Gennes. As far as the angular position of the intensity peak is concerned, our results agree well with de Gennes's prediction, as seen in Fig. 6, and hence equally well with Leibler's prediction. The gradual decrease in the peak intensity over a temperature range, as shown in Fig. 3, also agrees qualitatively with his prediction. It does not, however, agree quantitatively. He predicts $1/I_{max}$ to be linear with χ. For the styrene-butadiene pair χRT is nearly independent of temperature (as shown in our earlier study[14] on the miscibility of polystyrene and polybutadiene). When $1/I_{max}$ is plotted against $1/T$, however, our result turns out far from being linear. As will be discussed shortly, our data are better represented by a linear relation between $\log I_{max}$ and $1/T$. The SAXS pattern predicted by his theory above the transition temperature arises from the dynamic density fluctuation present in a disordered, essentially homogeneous liquid, and would exhibit no fine structure. Our SAXS patterns shown in Figs. 4 and 5 display a second (and a third) peak at low temperatures, indicating the presence of ordered arrays of microdomains, which however is not regular enough to give sharp peaks as his theory suggests. The theory predicts that for a diblock copolymer with a block length ratio of 1 to 3, the transition should occur when χN is equal to about 17, where N is the total number of equivalent segments in a block copolymer molecule. If V_{ref} is the volume of an equivalent segment, one can write

$$N = M v_{sp}/V_{ref} \tag{24}$$

and

$$\chi = \Lambda V_{ref}/RT \qquad (25)$$

where M is the molecular weight, v_{sp} the specific volume and Λ the polymer-polymer interaction parameter[14] in units of energy per unit volume. The product χN is then equal to $(\Lambda/RT)\, M\, v_{sp}$, the latter containing only experimentally measurable quantities. In our previous study[14], the interaction parameter Λ for styrene-butadiene was found to be about 0.7 cal/cm^3 at 150°C. With v_{sp} taken as 1 cm^3/g, the transition temperature predicted by Leibler's theory is 576°K, which is about 1.5 times 373°K (100°C), the temperature around which we believe our diblock copolymer sample loses its microdomain structure. Since no adjustable parameters are involved in this comparison, the agreement could be considered fairly good.

The transition we observe in this work is an equilibrium phenomenon, which is thermally reversible and independent of the thermal schedule of measurements as long as the sample is not exposed to excessibly high temperature. Moreover, the reorganization of the structure following any temperature change occurs very rapidly, indicating that the molecular motions involved are of a relatively short range. The rapidity of the structural reorganization was attested by our failure to quench the disordered structure. When a thin film sample of either block copolymer was heated to above 250°C and immediately dipped into ice water or liquid nitrogen, the SAXS pattern obtained at room temperature from the quenched film was very similar (showing only a moderate reduction in the peak intensity) to what were obtained with slow temperature changes. This is surprising in view of the fact that the glass transition temperature observed with our samples is around 80°.

The change in the SAXS pattern with temperature, observed in this work, closely resembles those changes widely observed during the kinetic process of spinodal decomposition of an unstable homogeneous solution into two separate phases. According

to the linear approximation theory[41-44] by Cahn and others, the intensity I(s,t) of scattering at successive time t from a supersaturated solution undergoing spinodal decomposition is given by

$$I(s,t) = I(s,0)\, e^{2R(s)t} \qquad (26)$$

where R(s) is the "amplification" factor denoting the rate at which the particular Fourier component associated with s grows with progress of the decomposition. R(s) goes through a maximum with increasing s and eventually becomes negative. As a result the SAXS patterns[45] obtained at successive times retain the same shape and the same peak position, while there exists an angle s_c at which all the curves cross each other. Figs. 1 and 2 show that our results, obtained at different temperatures, reproduce all the features, mentioned above, which are expected at different times in spinodal decomposition. In our results for both the di-block and triblock copolymers, the curves cross each other at around $s_c = 0.006\mathring{A}^{-1}$, which is about 1.5 times the peak angle $s_m \approx 0.004\mathring{A}^{-1}$. The ratio 1.5 agrees well with $\sqrt{2}$ predicted by Cahn[41,42] for a similar ratio in the case of spinodal decomposition. There are some further analogy we can draw between our results and the spinodal decomposition. The shapes of our SAXS intensity curves are all similar to each other. In Fig. 15 the peak intensity $\tilde{I}(s_m)$, divided by $(\Delta\rho)^2$ to correct for the change in the electron density difference between PS and PBD with temperature, is plotted against 1/T. A fairly good linear correlation between $\ln \tilde{I}(s_m)$ and 1/T is found. If some reasonable correction is made for the background and especially for the component of scattering rising rapidly as $s \to 0$, the linear correlation would extend to higher temperatures than seen in Figure 15. In analogy to eq. (26), the following empirical equation might then be adopted to represent our data approximately.

$$\tilde{I}(s, \chi) = \tilde{I}(s,0)\, e^{a(s)\chi} \qquad (27)$$

where the factor a(s) exhibits a maximum at s_m and a zero at s_c, the ratio

s_m/s_c being about 1.5.

The similarity between the two equations (26) and (27) underscores the rather surprising resemblence between the two, very different processes, one kinetic and the other thermodynamic. In our system, as an equilibrium is attained at each new temperature, the morphology attained must be very similar to what is achieved momentarily at various intermediate stages of spinodal decomposition. The amplification factor R(s) in Cahn's theory is given by

$$R(s) = Ms^2 (-F''-2K s^2) \qquad (28)$$

where M is the diffusion coefficient, F'' is the second derivative of the free energy with respect to concentration and K is a constant denoting the interaction between foreign neighbors. F'' is negative for an unstable mixture undergoing spinodal decomposition, while K is positive (unfavorable foreign interaction) for any system which eventually separates into two phases. The growth of density inhomogeneity of long wave lengths (small s) is limited by the diffusion process, as expressed by the factor Ms^2 in (28). The growth of inhomogeneity of short wave lengths (large s) is on the other hand opposed by the accompanying increase in the interfacial free energy, as expressed by the term $2Ks^2$. In the block copolymer system, it could be speculated that the relative stability (at equilibrium) of density inhomogeneity of different wave lengths is again governed by an expression similar to (28). The factor $(-F''-2K s^2)$ has its origin in the thermodynamic theory[46] of inhomogeneous liquid mixtures. The physical basis embodied in this theory probably applies to our present system as well, and gives rise to the same factor $(-F'' - 2K s^2)$ as governing the stability of density inhomogeneity at equilibrium. The front factor Ms^2 might also be replaced by a similar factor expressing the fact that a cluster of same segments much larger than the molecular dimension is difficult to form. Since the shape of polymer molecules can often be represented by a diffusion equation, it might even

be possible that this geometric effect gives rise to a factor proportional to s^2. If there is any validity in the above conjecture, then the relative stability a(s) indeed could be represented approximately by an expression similar to (28), and the agreement of the observed ration s_c/s_m with the theoretical value of $\sqrt{2}$ may not entirely be a coincidence.

The same triblock copolymer sample investigated here was earlier studied rheologically by two groups[10,11] of workers, and was shown on raising the temperature to exhibit a distinct change in the flow properties, from a Newtonian to a non-Newtonian behavior, in the interval between 140 and 165°C. Our SAXS results, however, do not show any corresponding discontinuity. The desmeared SAXS patterns given in Fig. 5 show that the fine structure in the intensity pattern, indicative of an ordered structure in the sample, seems to disappear in this temperature range. It does not necessarily follow from it, however, that the observed rheological transition coincides with the thermodynamic transition. The latter is a weak transition, at which only the last remaining trace of microdomains finally disappears (at temperature T_A in Fig. 14), and may not be accompanied by any discontinuity in normally observable bulk properties. There is a possible alternative explanation for the rheological discontinuity. In a triblock copolymer at temperatures far below the transition point, the two styrene blocks belonging to a single molecule are in most cases incorporated in two different microdomains, thus making the intervening butadiene block to serve as a bridge connecting the domains. Some small fraction of the molecules would, however, have their two styrene blocks in the same microdomain, thus failing to contribute their butadiene blocks to the formation of the network structure. The non-bridging molecules, with the end-to-end distance of the butadiene block substantially shorter, have a higher entropy than the bridging molecules. As a result, as the temperature is raised, the number of the bridging molecules will dwindle more rapidly than the

non-bridging ones, until eventually the sample as a whole behaves no longer as a network material, although the microdomains, now much reduced in size, may still remain. If the above view is correct, a diblock copolymer sample would not exhibit a similar rheological discontinuity in the comparable temperature range.

Finally, comparison is made here between the results obtained with the diblock and triblock copolymers. The difference between the two are minor, and most of the qualitive features discussed above apply equally to both. The main observed difference is that the temperature range of transition for the triblock copolymer is higher by about 90°. This is qualitatively in agreement with the analysis recently given by Bauer and Fetters[47]. It shows that the loss of entropy resulting from joining two diblock copolymer molecules to form a triblock molecule is more severe in the disordered phase than in the structure containing microdomains. No quantitative theory is at present available, however, to compare with our observed difference of 90°.

The unperturbed end-to-end distances of a polystyrene molecule of mol. wt. 7000, a polybutadiene of 21000 and a polybutadiene of 43000 are estimated to be 57, 130 and 187 Å respectively. The end-to-end distances of the diblock and triblock copolymer molecules in our samples are then estimated to be 142 and 203 Å respectively. The interdomain distances determined from the angular positions of the main SAXS peaks are 205 and 214 Å for the diblock and triblock copolymer samples respectively (see Table I). The interdomain distance for the triblock copolymer sample agrees well with its end-to-end distance, suggesting that the conformation of the molecules is not much distorted from their unperturbed states, and that the requirement of the segment density constancy in space is not a very severe constaint. The increased freedom allowed to a diblock molecule apparently does not bring about any appreciable change in the morphology.

Acknowledgment

This work was supported in part by the Office of Naval Research. We gratefully acknowledge helpful discussions with Drs. C. I. Chung, W. Ruland, E. W. Fischer and L. Leibler.

Appendix

The density profile across the interface between two phases of density ρ_1 and ρ_2 can be written as

$$\rho(x) = q(x)\ (\rho_1 - \rho_2)/2 + (\rho_1 + \rho_2)/2\ . \qquad (A1)$$

When the distance x is measured from the center of the diffuse boundary, the profile function q(x) is likely to have

$$q(0)=0;\quad q(-x)= -q(x);\quad q(x)=1 \qquad (A2)$$

The following form of q(x) was derived by Cahn and Hilliard[46] in their theory of inhomogeneous liquid systems:

$$q(x) = \tanh(2x/t) \qquad (A3)$$

where t is a measure of the thickness of the diffuse interface. The same expression (A3) was later obtained by other workers in the theories[48-51] of polymer-polymer mixtures and block copolymers. Several quantities of interest in SAXS which follow from (A3) are derived here.

In an ideal two phase system with sharp boundaries, the invariant Q or the mean square deviation of the electron density from its mean is given by

$$\langle(\delta\rho)^2\rangle_0 = (\Delta\rho)^2\phi_1\phi_2 \qquad (A4)$$

where $\Delta\rho = \rho_1 - \rho_2$. For a two phase system, otherwise idential to the above but with diffuse boundaries, the mean square electron density deviation becomes

$$\langle(\delta\rho)^2\rangle = (\Delta\rho)^2\ \phi_1\phi_2 - \frac{(\Delta\rho)^2}{2}\ \frac{S}{V}\int_o^\infty [1 - q^2(x)]\ dx \qquad (A5)$$

where S/V is the specific area of the boundary. (It is assumed here that the interface thickness is small compared to the radius of curvature of the interface). With (A3) for q(x), (A5) becomes

$$\langle(\delta\rho)^2\rangle = (\Delta\rho)^2\ \phi_1\phi_2 - (\Delta\rho)^2\ (S/V)\ (t/4) \qquad (A6)$$

$$= (\Delta\rho)^2\ \phi_1\phi_2\ \ (1 - t/l_p) \qquad (A7)$$

where $l_p = 4\ (V/S)\ \phi_1\phi_2$ is Porod's length of inhomogeneity. Thus the fractional reduction in the invariant due to diffuse boundaries can be written as

$$y \equiv 1-Q/Q_0 = t/l_p \ . \tag{A8}$$

Next we examine the effect of diffuse boundaries on SAXS intensity. As discussed by Ruland[35], the electron density ρ in the system having diffuse boundaries can be represented by a convolution product of the electron density ρ_0 in an ideal two phase system with a smoothing function h, so that

$$\rho = \rho_0 * h \ . \tag{A9}$$

The intensity scattered from the system having diffuse boundaries is then given by

$$I = I_0 \cdot H^2 \tag{A10}$$

where H is the Fourier transform of h and I_0 is the intensity scattered from the ideal two-phase material. We therefore seek a smoothing function h which, when convoluted with a step function, will produce eq. (A3), i.e.,

$$\mathrm{sgn}(x) * h(x) = \tanh\ (2x/t) \tag{A11}$$

where sgn(x) = -1 for x<0 and sgn(x) = 1 for x>0. Since[52]

$$\mathcal{F}\{\mathrm{sgn}(x)\} = -i/\pi s \tag{A12}$$

and

$$\mathcal{F}\{\tanh(2x/t)\} = -i(\pi t/2)\ \mathrm{csch}\ (\pi^2 ts/2) \tag{A13}$$

we obtain

$$\mathcal{F}\{h(x)\} \equiv H(s) = (\pi^2 ts/2)\ \mathrm{csch}\ (\pi^2 ts/2) \tag{A14}$$

and

$$h(x) = (1/t)\ \mathrm{sech}^2\ (2x/t). \tag{A15}$$

Hence, in the Porod's region, the observed intensity (in electron unit per unit volume of the sample) will approach as s increases to

$$I(s) \sim \frac{(\Delta\rho)^2}{8\pi^3} \frac{S}{V} \frac{1}{s^4} H^2(s) \qquad \text{(A16)}$$

The variance σ^2 of the function $h(x)$ is

$$\sigma^2 = (\pi^2/48)\, t^2 \qquad \text{(A17)}$$

so that $H^2(s)$ can be written as

$$H^2(s) = (\pi\sqrt{12}\,\sigma s)^2 \operatorname{csch}^2 (\pi\sqrt{12}\,\sigma s) \qquad \text{(A18)}$$

$$\approx 1 - 4\pi^2\sigma^2 s^2 + \ldots\ldots \qquad \text{(A19)}$$

In the expansion of $H^2(s)$, the second order term is identical to the one in the similar expansion of eq. (6) based on a gaussian smoothing function. The "effective" thickness t is related to the slope of q(x) function (A3) by

$$t = 2/q'(0). \qquad \text{(A20)}$$

The "effective" thickness may be defined in the same way even when the interface profile is given by another function. For a gaussian smoothing function, we then have

$$\sigma^2 = (1/2\pi)\, t^2_{\text{gauss}}. \qquad \text{(A21)}$$

Comparison of (A21) with (A17) shows that, when interfacial concentration profiles having the same slope at x = 0 is compared, the one following eq. (A3) approaches to the limiting density with increasing x much more slowly than the one associated with a gaussian smoothing function, as pointed out graphically by Hashimoto et al[26].

REFERENCES

1. D. J. Meier, J. Polymer Sci., Part C, 26, 81 (1969)

2. D. J. Meier, in "Block and Graft Copolymers," J. J. Burke and V. Weiss, Eds., Syracuse University Press, Syracuse, NY, 1973

3. D. J. Meier, Polymer Prepr., Am. Chem. Soc., Div. Polymer Chem., 15, 171 (1974)

4. S. Krause, Macromol., 3, 84 (1970)

5. D. F. Leary and M. C. Williams, J. Polymer Sci., Polymer Phys. Ed., 11, 345 (1973)

6. E. Helfand and Z. R. Wasserman, Macromol., 9, 879 (1976); 11, 960 (1978)

7. E. Helfand and Z. R. Wasserman, Polymer Eng. Sci., 17, 535 (1977)

8. R. E. Boehm and W. R. Krigbaum, J. Polymer Sci., 54C, 153 (1976)

9. L. Leibler, Macromol., 13, 1602 (1980)

10. C. I. Chung and J. C. Gale, J. Polymer Sci., Polymer Phys. Ed., 14, 1149 (1976)

11. E. V. Gouinlock and R. S. Porter, Polymer Eng. Sci., 17, 534 (1977)

12. D. F. Leary and M. C. Williams, J. Polymer Sci., Polymer Phys. Ed., 12, 265 (1974)

13. A. R. Ramos and R. E. Cohen, Polymer Eng. Sci., 17, 639 (1977)

14. R. J. Roe and W. C. Zin, Macromol., 13, 1221 (1980)

15. C. I. Chung, H. L. Griesback, and L. Young, J. Polymer Sci., Polymer Phys. Ed., 18, 1237 (1980)

16. R. J. Roe, J. C. Chang, M. Fishkis, and J. J. Curro, J. Appl. Crys. in press

17. O. Kratky, I. Pilz, and P. J. Schmitz, J. Colloid Interface Sci., 21, 24 (1966)

18. E. Campos-Lopez, D. McIntyre, and L. J. Fetters, Macromol., 6, 415 (1973)

19. A. Todo, H. Uno, K. Miyoshi, T. Hasimoto, and H. Kawai, Polymer Eng. Sci., 17, 587 (1977)

20. A. Todo, T. Hashimoto, and H. Kawai, J. Appl. Cryst., 11, 558 (1978)

21. M. Fujimura, H. Hashimoto, K. Kurahashi, T. Hashimoto, and H. Kawai, unpublished manuscript.

22. P. G. de Gennes, J. Phys. (Paris), 31, 235 (1970)

23. A. D. LeGrand and D. G. LeGrand, Macromol., 12, 450 (1979)

24. G. Kortleve, C. A. F. Tuynman, and C. G. Vonk, J. Polymer Sci. A2, 10, 123 (1972)

25. C. G. Vonk, J. Appl. Cryst., 6, 81 (1973)

26. T. Hashimoto, M. Shibayama, and H. Kawai, Macromol., 13, 1237 (1980)

27. A. Guinier, "X-ray Diffraction," Freeman and Co., San Francisco, 1963

28. P. A. Egelstaff, "An Introduction to the Liquid State," Academic Press, New York, 1967

29. F. Kohler, "The Liquid State," Verlag Chemie, Weinheim, Germany, 1972

30. J. J. Curro and R. J. Roe, unpublished results

31. J. H. Wendorff and E. W. Fischer, Koll-Z. u. Z. Polym., 251, 876 (1973)

32. J. Rathje and W. Ruland, Colloid Polym. Sci., 254, 358 (1976)

33. A. L. Renninger and D. R. Uhlmann, J. Polymer Sci., Polymer Phys. Ed., 13, 1481 (1975); 14, 415 (1976); 16, 2237 (1978)

34. M. K. Lee and R. J. Roe, unpublished results

35. W. Ruland, J. Appl. Cryst., 4, 70 (1971)

36. W. Ruland, J. Appl. Cryst., 1, 383 (1974)

37. J. .. Koberstein, B. Morra, and R. S. Stein, J. Appl. Cryst., 13, 34 (1980)

38. T. Hashimoto, A. Todo, H. Itoi and H. Kawai, Macromol., 10, 377 (1977)

39. Th. G. Scholte, J. Polymer Sci., A2, 9, 1553 (1971)

40. B. Chu, R. J. Schoenes, and M. E. Fischer, Phys. Rev., 185, 219 (1969)

41. J. W. Cahn, Acta Metal., 9, 795 (1961)

42. J. W. Cahn, J. Chem. Phys., 42, 93 (1965)

43. J. W. Cahn, Trans. Metal. Soc. AIME, 242, 166 (1968)

44. H. E. Cook, Acta Metal., 18, 297 (1970)

45. V. Gerold and G. Kostorz, J. Appl. Cryst., 11, 376 (1978)

46. J. W. Cahn and J. E. Hilliard, J. Chem. Phys., 28, 258 (1958)

47. B. J. Bauer and L. J. Fetters, Macromol., 13, 1027 (1980)

48. R. J. Roe, J. Chem. Phys., 62, 490 (1975)

49. E. Helfand and Y. Tagami, J. Chem. Phys., 62, 1327 (1975)

50. E. Helfand, Acc. Chem. Res., 8, 295 (1975)

51. R. W. Hopper and D. R. Uhlmann, J. Colloid Interface Sci., 47, 77 (1974)

52. R. N. Bracewell, "The Fourier Transform and Its Applications," 2nd Ed., McGraw-Hill, New York, 1978

TABLE I

Scattering Peak Positions and Structural Features Deduced from Them

	Diblock Copolymer	Triblock Copolymer
Peak angles s ($\mathring{A}^{-1}$)	0.0049, 0.0079, 0.0131	0.0047, 0.0077, 0.0119
Interdomain distance D ($\mathring{A}$)	205	214
Radius of spherical domain a ($\mathring{A}$)	70	77

TABLE II

Least Squares Evaluation of Interface Thickness Parameter σ and Porod's Length of Inhomogeneity l_p

Sample	Temp	σ (Å)	l_p (Å^{-1})	Angular Range (Å^{-1})
Diblock Copolymer	20°C	4.4 ± 0.5	43 ± 5	0.026 - 0.060
	75	4.5 ± 1.0	27 ± 6	0.029 - 0.060
	100	4.2 ± 0.6	25 ± 3	0.029 - 0.060
	170	3.5 ± 0.8	19 ± 4	0.029 - 0.060
	200	3.6 ± 1.5	17 ± 6	0.029 - 0.060
Triblock Copolymer	20°C	6.3 ± 0.2	75 ± 3	0.013 - 0.060
	140	5.6 ± 0.7	44 ± 6	0.018 - 0.060
	170	3.5 ± 1.3	43 ± 9	0.019 - 0.060

LEGEND TO FIGURES

Figure 1. The slit-smeared intensity $\tilde{I}(s)$, obtained with the diblock copolymer sample, is plotted against the scattering angle s (= 2 sin θ/λ). The curves show the data obtained at 20°, 75°, 100°, 125°, 140°, 170°, 200°, and 246°C.

Figure 2. The slit-smeared intensity $\tilde{I}(s)$, obtained with the triblock copolymer sample, is plotted against s. The curves show the data obtained at 20°, 100°, 140°, 176°, 200°, and 250°C in the order of decreasing peak intensity. Note that $\tilde{I}(s)$ is in linear scale here while it is in logarithmic scale in Fig. 1.

Figure 3. The intensity $\tilde{I}_{max}$ at the peak (from which the background is subtracted) is plotted against temperature. Circle: triblock copolymer. Square: diblock copolymer.

Figure 4. The desmeared intensity I(s) for the diblock copolymer sample is plotted against s. The curve for 20°C is given in electron unit per unit volume of sample, while the curves at successively higher temperatures are each displaced from the preceding one by a factor 0.1 in order to avoid overlapping.

Figure 5. The desmeared intensity I(s) for the triblock copolymer sample is plotted against s. The curve for 20°C is given in electron unit per unit volume of sample, while the curves at successively higher temperatures are each displaced from the preceding one by a factor 0.1 in order to avoid overlapping.

Figure 6. The desmeared intensity for the diblock copolymer obtained at 200°C, plotted with circles, is compared against the curve (in solid line) calculated according to de Gennes's theory[22] for a homogeneous diblock copolymer liquid. The positions of the peaks agree well, and also, if we assume a component of scattering rapidly rising toward angle zero as indicated by the broken line, the absolute magnitude of the intensity can be considered comparable.

Figure 7. The desmeared intensity for the diblock copolymer sample is plotted against s^6 to show that the empirical equation (1) is fairly well obeyed. Note that at higher temperatures, the deviation from eq. (1) persists to higher angles. The data for the triblock copolymer samples show very similar features.

Figure 8. The "background" intensity I(0), desmeared and extrapolated to angle zero, obtained with the diblock copolymer sample is plotted against temperature (open squares). Shown for comparison is the similar intensity I(0) obtained with polystyrene (filled circles), which is known to arise from the thermal density fluctuations present in amorphous materials.

Figure 9. The invariant Q, evaluated according to eq. (4), is plotted against temperature: squares for the diblock and triangles for the triblock copolymer samples. The solid curve is the invariant calculated for a block copolymer of the same composition but having an ideal two-phase structure. Its variation with temperature arises from the change in the electron-density contrast between polystyrene and polybutadiene, and the kink in the curve represents the glass transition of polystyrene.

Figure 10. The plot to evaluate the interfacial thickness parameter σ according to eq. (8). The data are for the diblock copolymer sample. $s\tilde{I}(s)$ (with $\tilde{I}$ from which the "background" $\tilde{I}_b$ has been subtracted) is plotted against s^{-2}. σ is then proportional to $(-\text{intercept/slope})^{\frac{1}{2}}$. For the sake of clarity, the data points for 100° and 200°C are displaced upward by 5 and 10 ordinate units, respectively.

Figure 11. The same data shown in Fig. 10 are presented in a different manner in order to evaluate the interfacial thickness parameter σ according to eq. (9). Here $s^{-1.81} \ln(s^3\tilde{I})$ (with $\tilde{I}$ from which the "background" $\tilde{I}_b$ has been subtracted) is plotted against $s^{-1.81}$. σ is then evaluated as (-inter-

cept/38)$^{1/1.81}$. For the sake of clarity the data points for 100° and 200°C are displaced upward by 2000 and 4000 ordinate units respectively.

Figure 12. Schematic representation of the possible models of intermediate structures during the transition. At low temperature the interface is only moderately diffuse, and components are fairly well segregated into their respective domains. At high temperature, the domain structure has disappeared and only random fluctuation of concentration remains. For the intermediate temperature, two extreme models are depicted. In Model I, the interface becomes more and more diffuse, but the center of the domains retain their original composition. In Model II the interface thickness remains about the same but intermixing of components results in reduced density contrast between the domains and also in a reduction in the size of the domains.

Figure 13. The shape factor of f(s) calculated by eq. (20). Curve 1 is for spherical domains of radius 70 Å and interface thickness 14 Å. Curve 2 is for radius 70 Å and interface thickness 42 Å as representing Model I in Fig. 12. Curve 3 is for radius 58.09 Å and interface thickness 14 Å, but the electron density contrast reduced to 0.875 times that of curves 1 and 2, and is meant to represent Model II in Fig. 12.

Figure 14. Schematic representation of the proposed changes in the composition of the two microphases with temperature. Curve 1 represents the concentration of styrene in the spherical domains, and remains largely unchanged. Curve 2 depicts the gradual dissolution of styrene into the butadiene matrix. At temperature T_A, the concentration of styrene in the matrix becomes equal to 25% and the domain structure disappears. The portion of the curve drawn light is never realized.

Figure 15. The peak intensity $\tilde{I}_{max}$ divided by the square of the electron density contrat $\Delta\rho$ at the respective temperature is plotted against 1/T, to show that eq. (27) might be a reasonable approximation to represent our data empirically.

Fig. 1

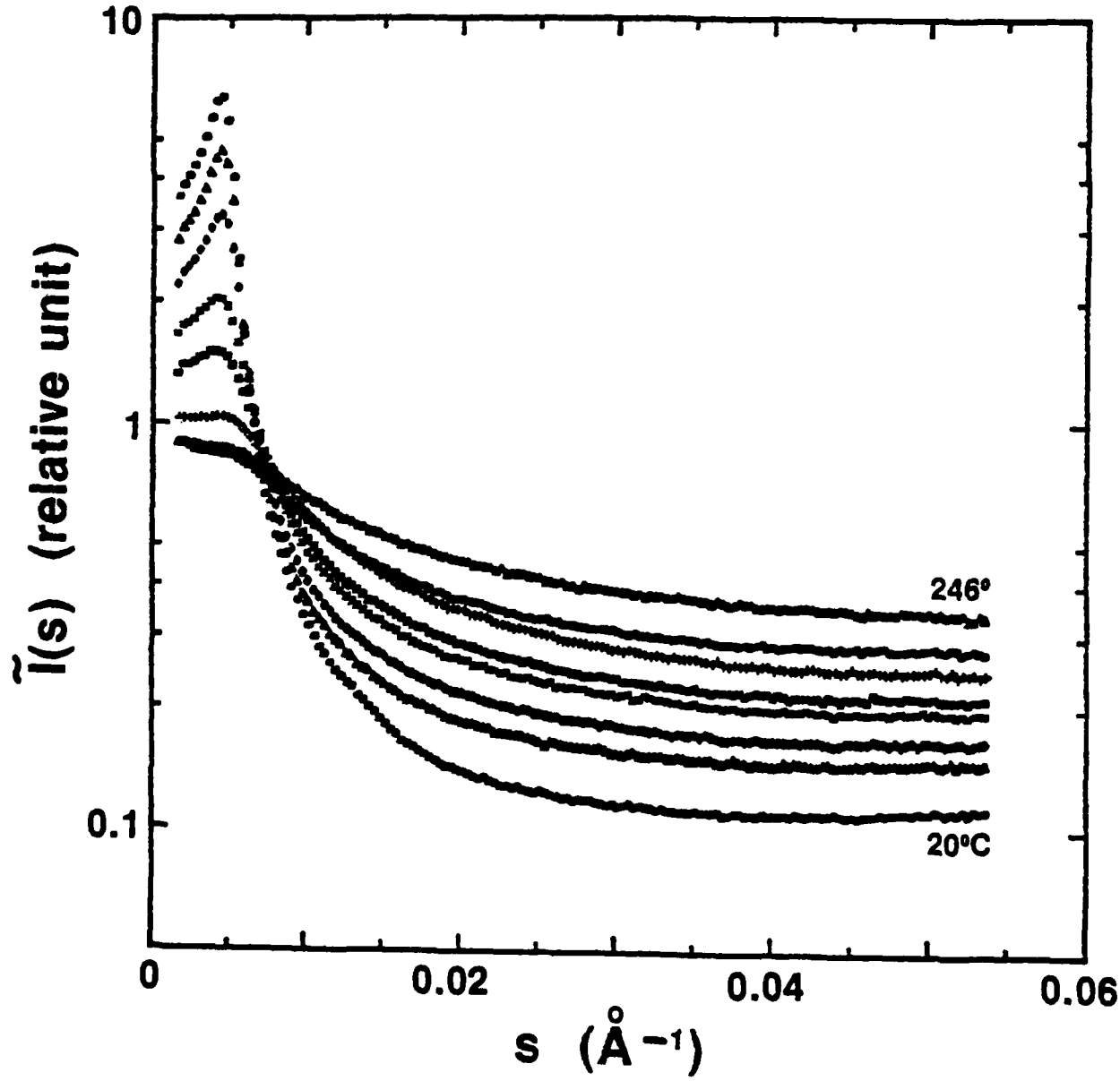

Fig. 2

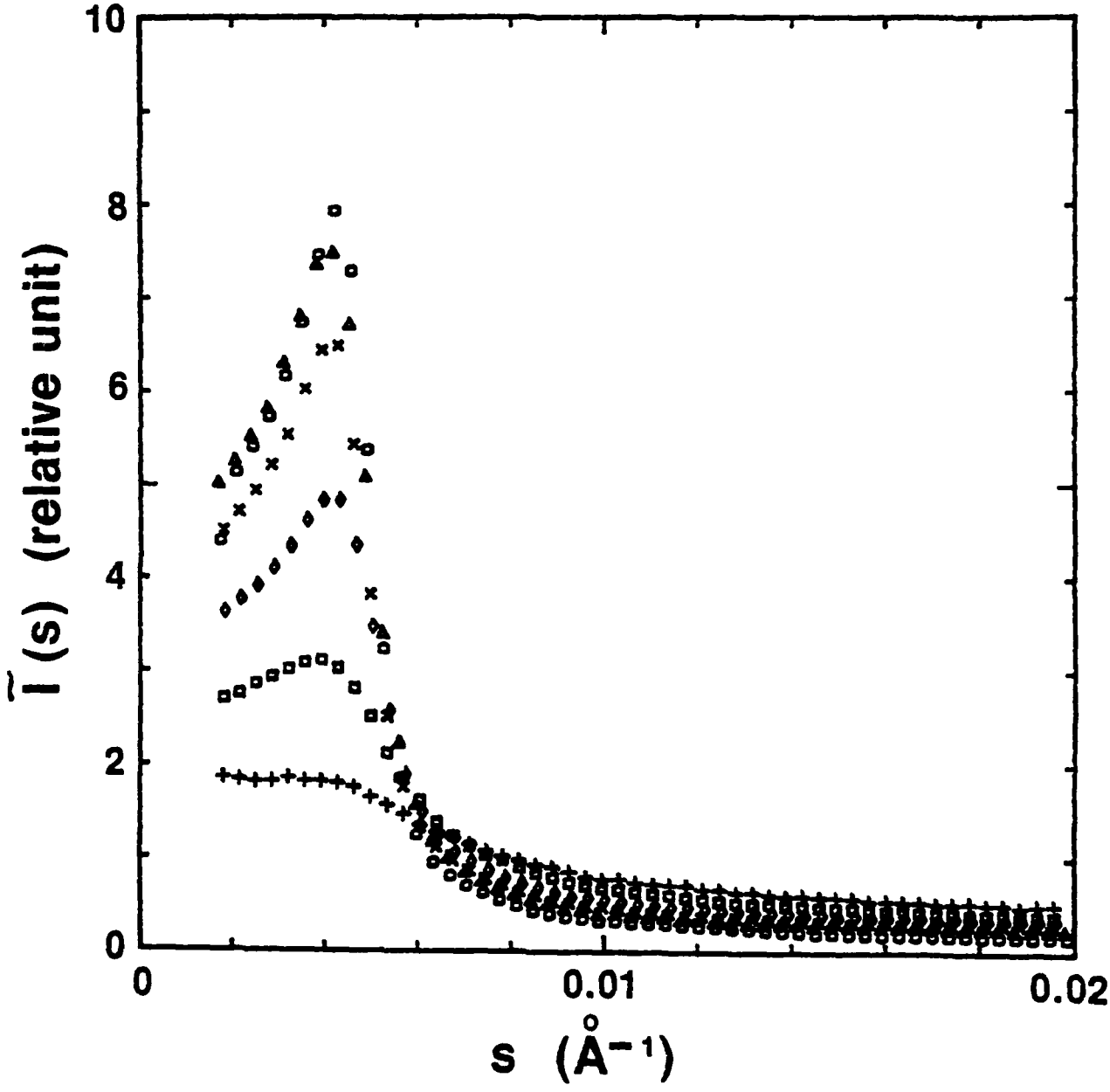

Fig. 3

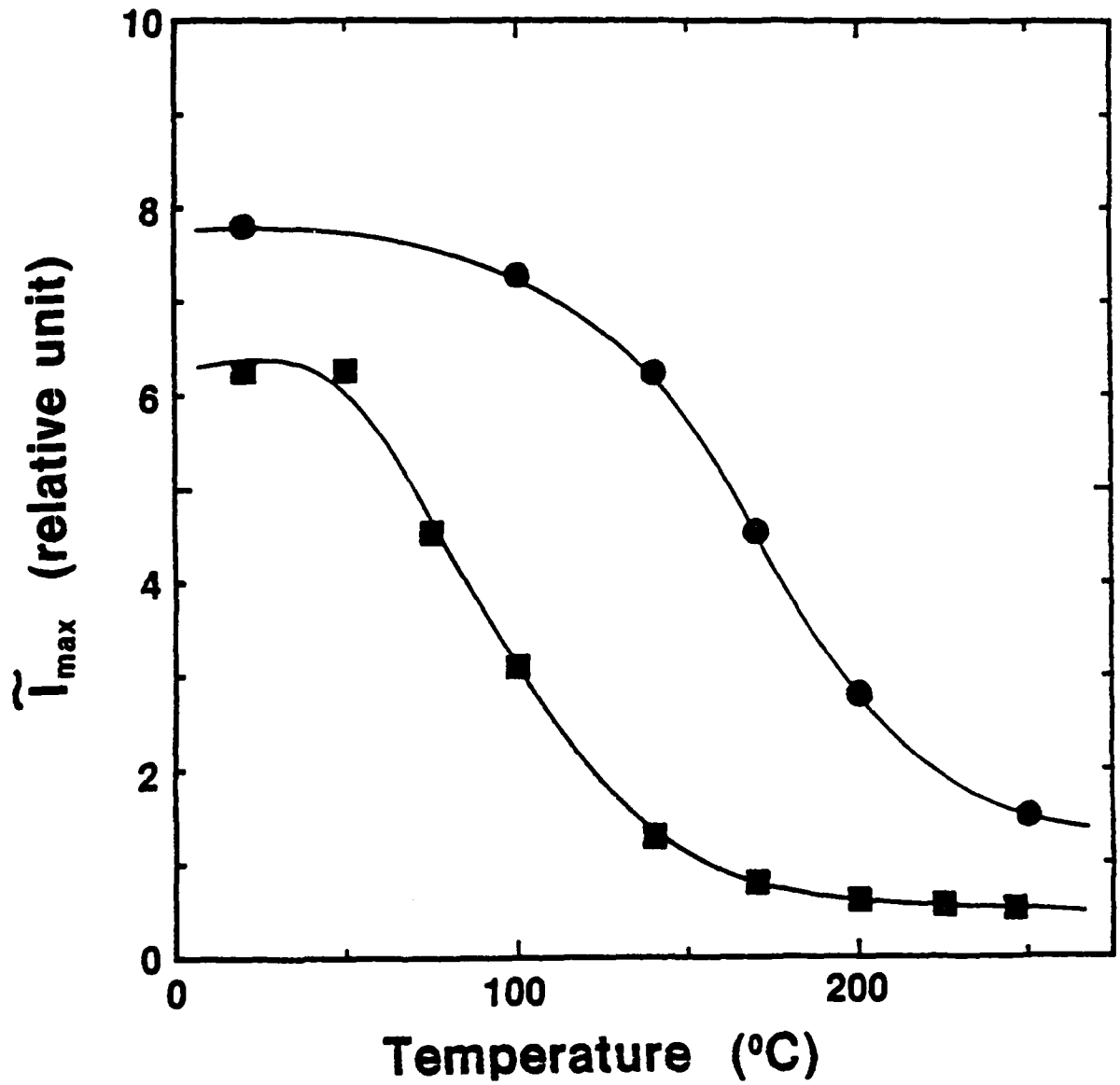

Fig. 4

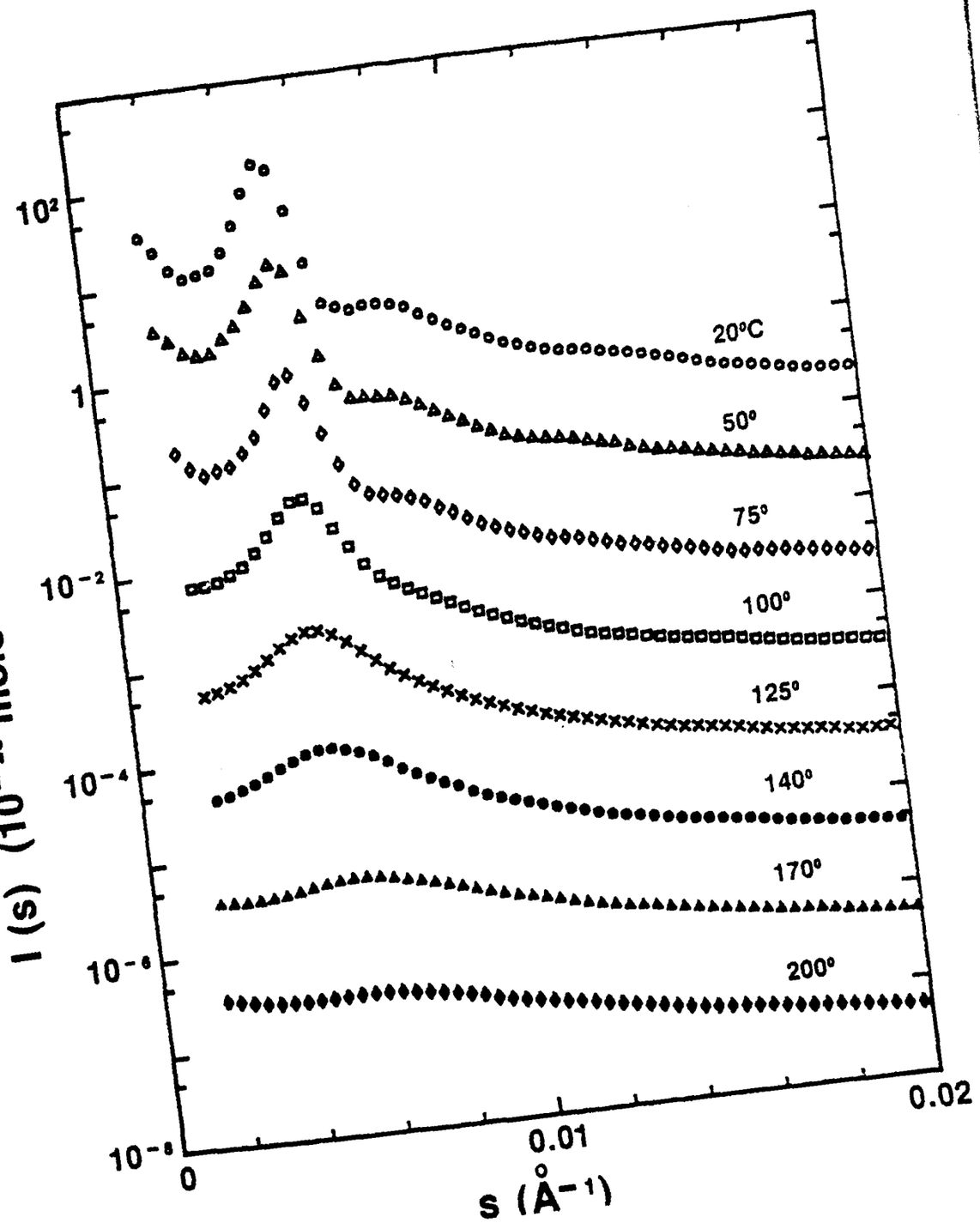
I (s) (10⁻²³ mole-electron²/cm³)
10²
1
10⁻²
10⁻⁴
10⁻⁶
10⁻⁸
0
0.01
0.02
s (Å⁻¹)
20°C
50°
75°
100°
125°
140°
170°
200°

Fig. 5

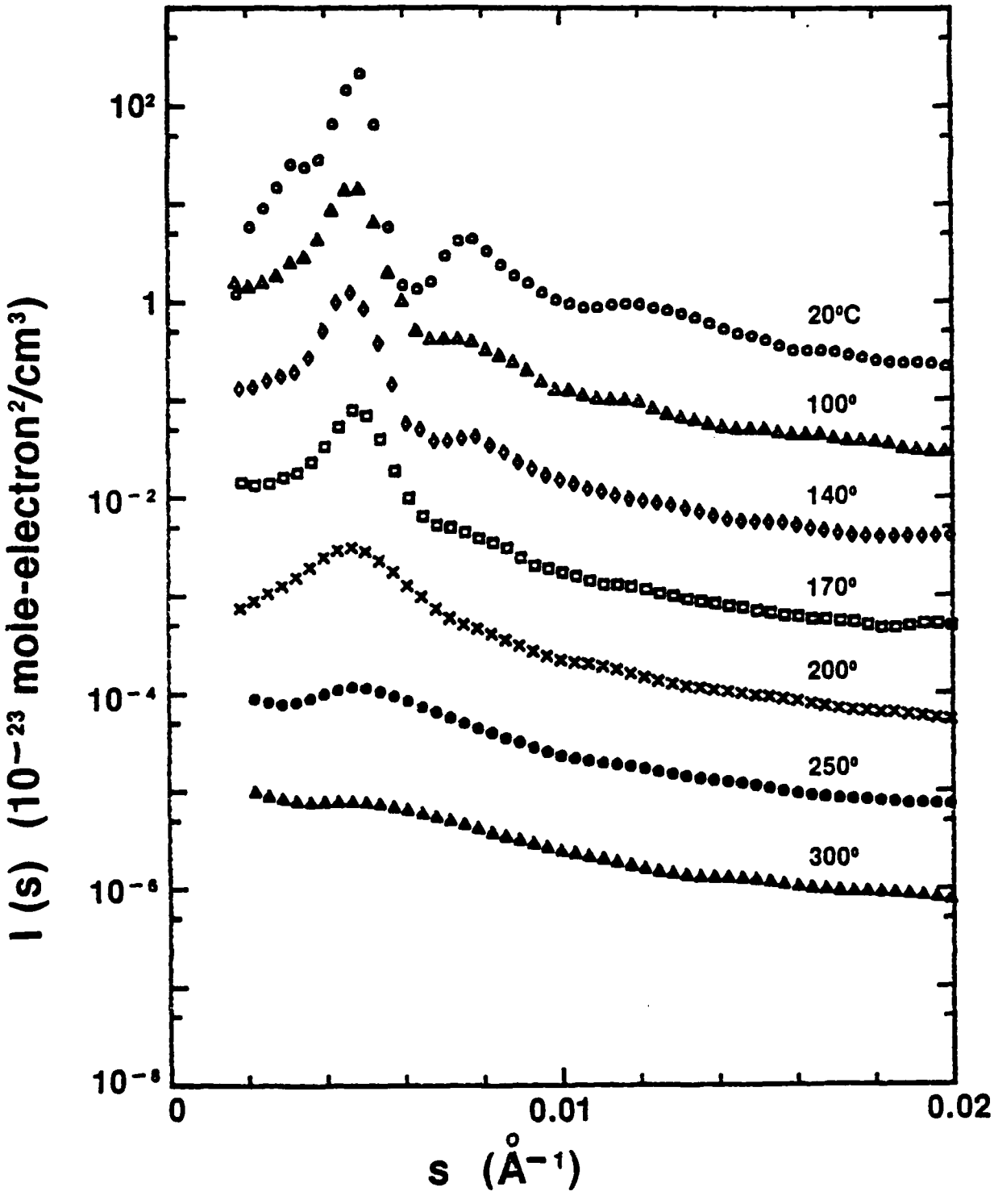
10^2
1
10^{-2}
10^{-4}
10^{-6}
10^{-8}
I (s) (10^{-23} mole-electron^2/cm^3)
0
0.01
0.02
s (Å^{-1})
20°C
100°
140°
170°
200°
250°
300°

Fig. 6

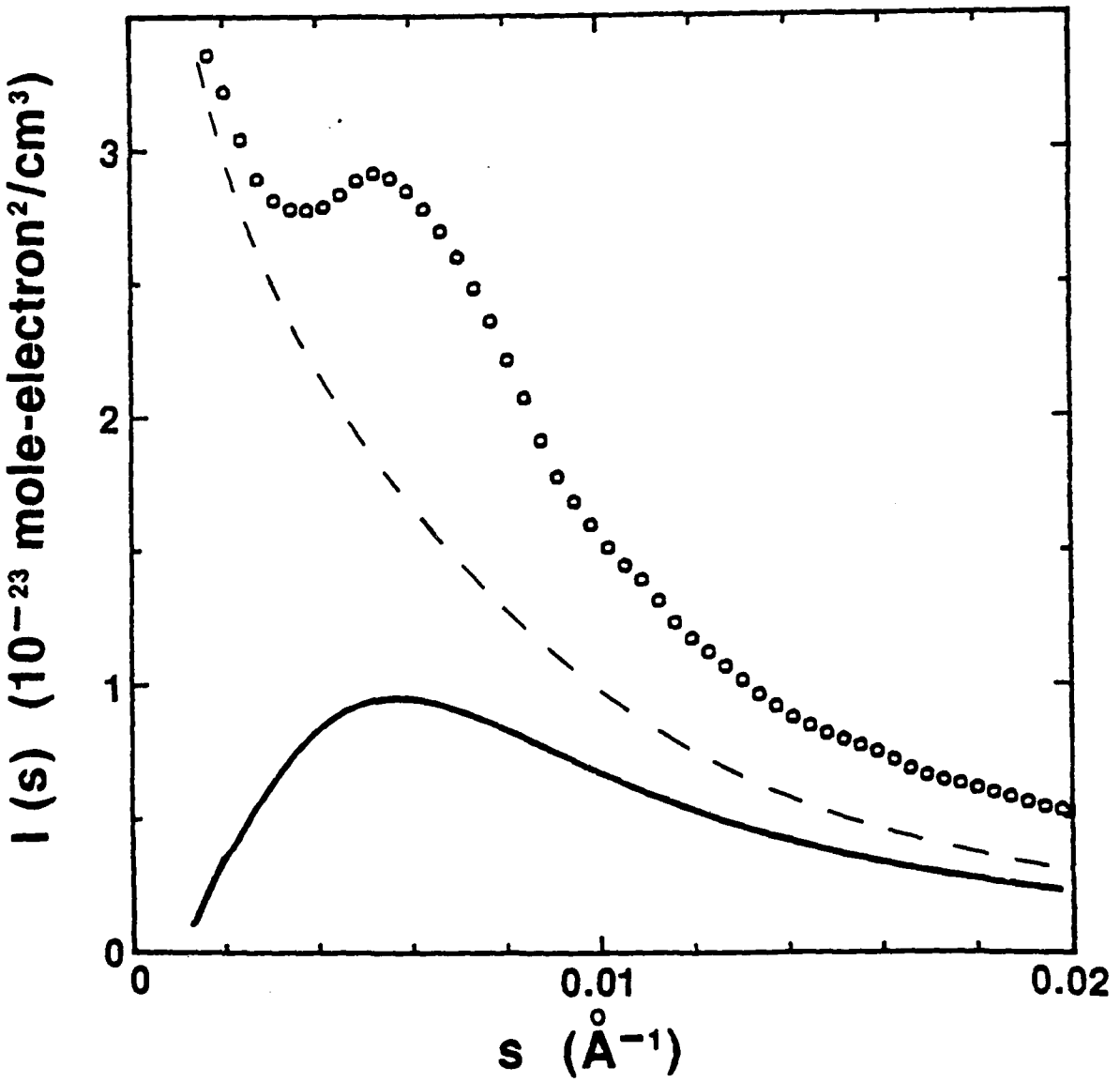

Fig. 7

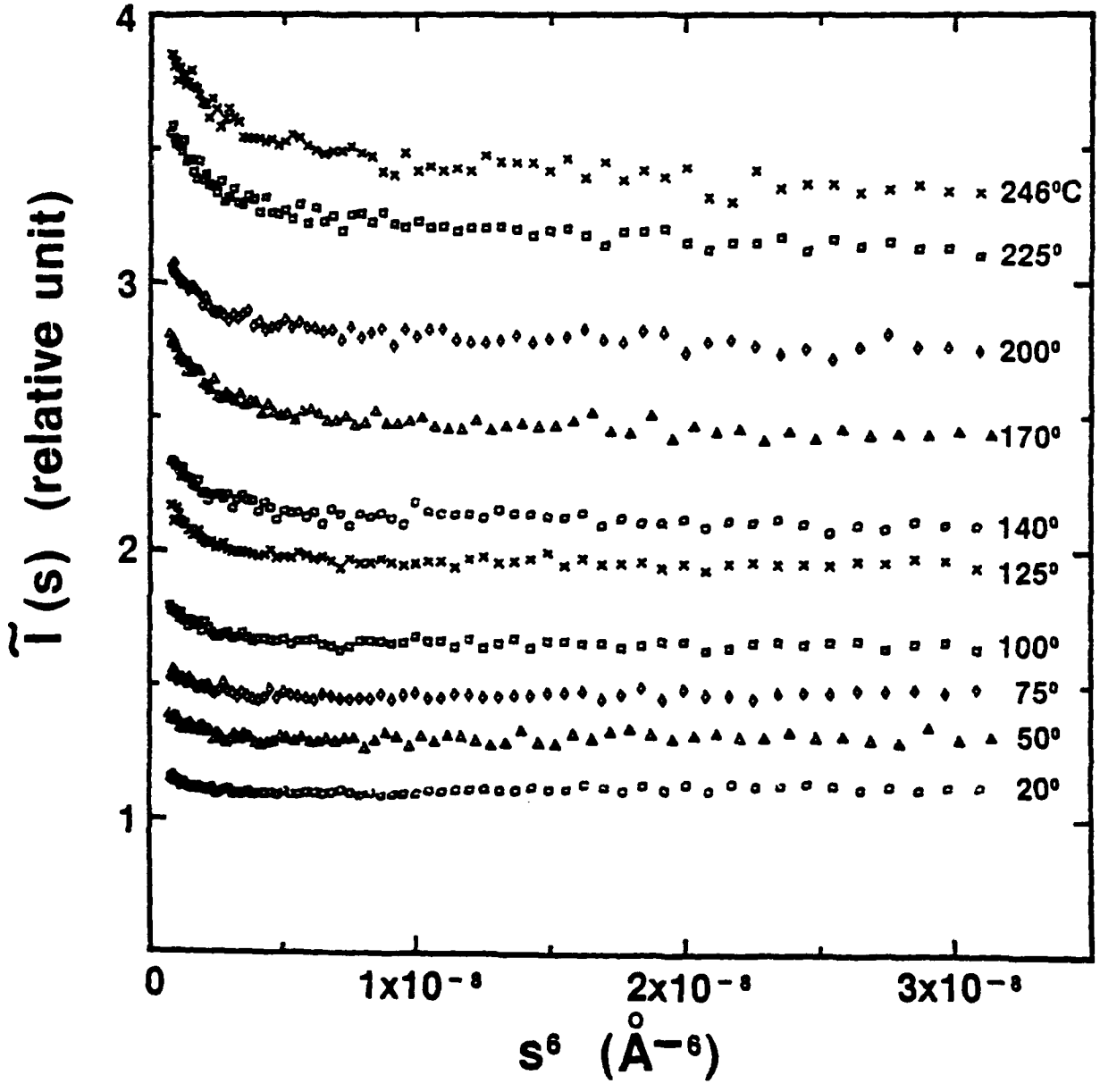
4
3
2
1
0
1x10⁻⁸
2x10⁻⁸
3x10⁻⁸
s⁶ (Å⁻⁶)
Ĩ (s) (relative unit)
246°C
225°
200°
170°
140°
125°
100°
75°
50°
20°

Fig. 8

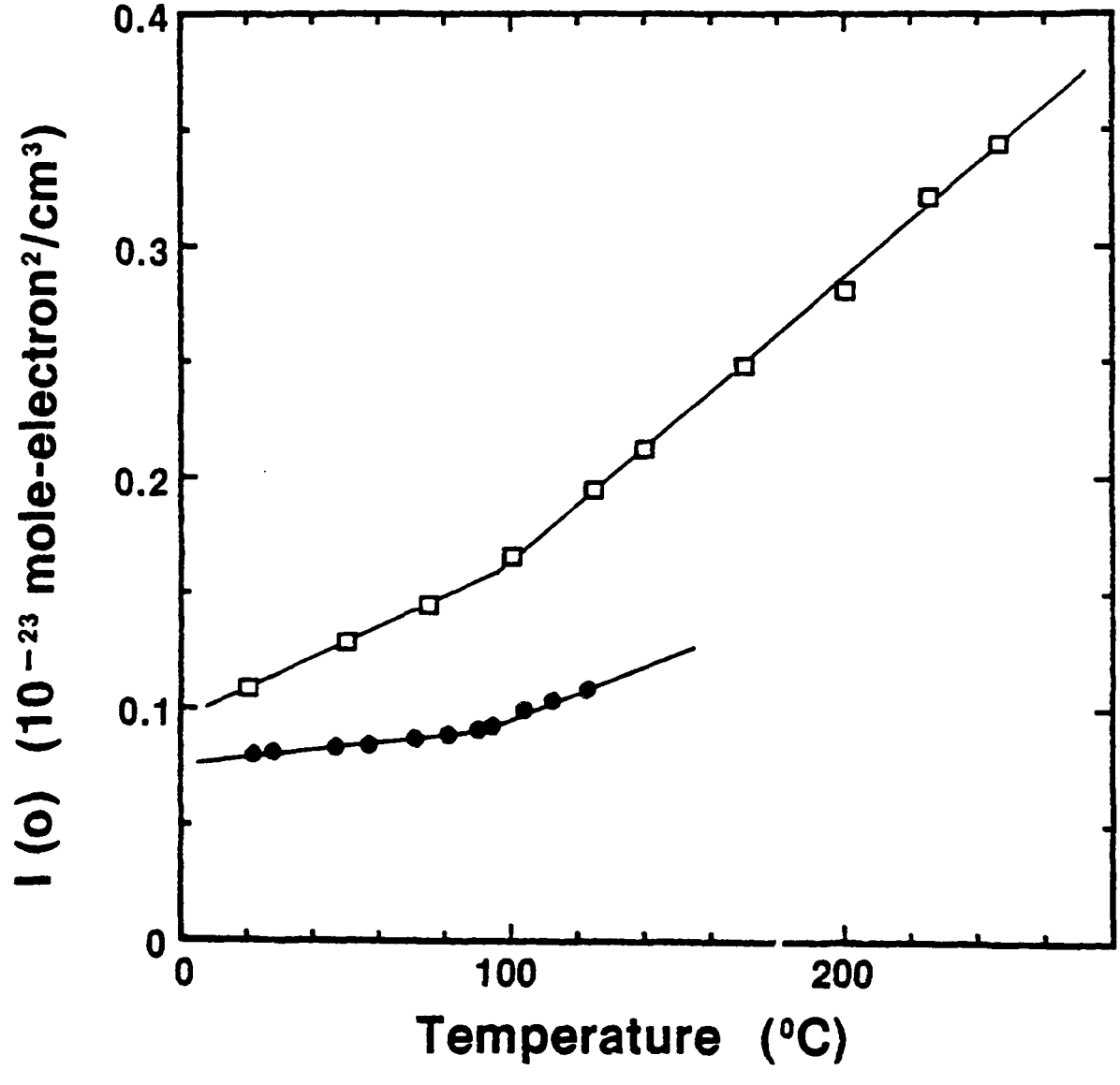
0.4
0.3
0.2
0.1
0
0
100
200
I (o) (10⁻²³ mole-electron²/cm³)
Temperature (°C)

Fig. 9

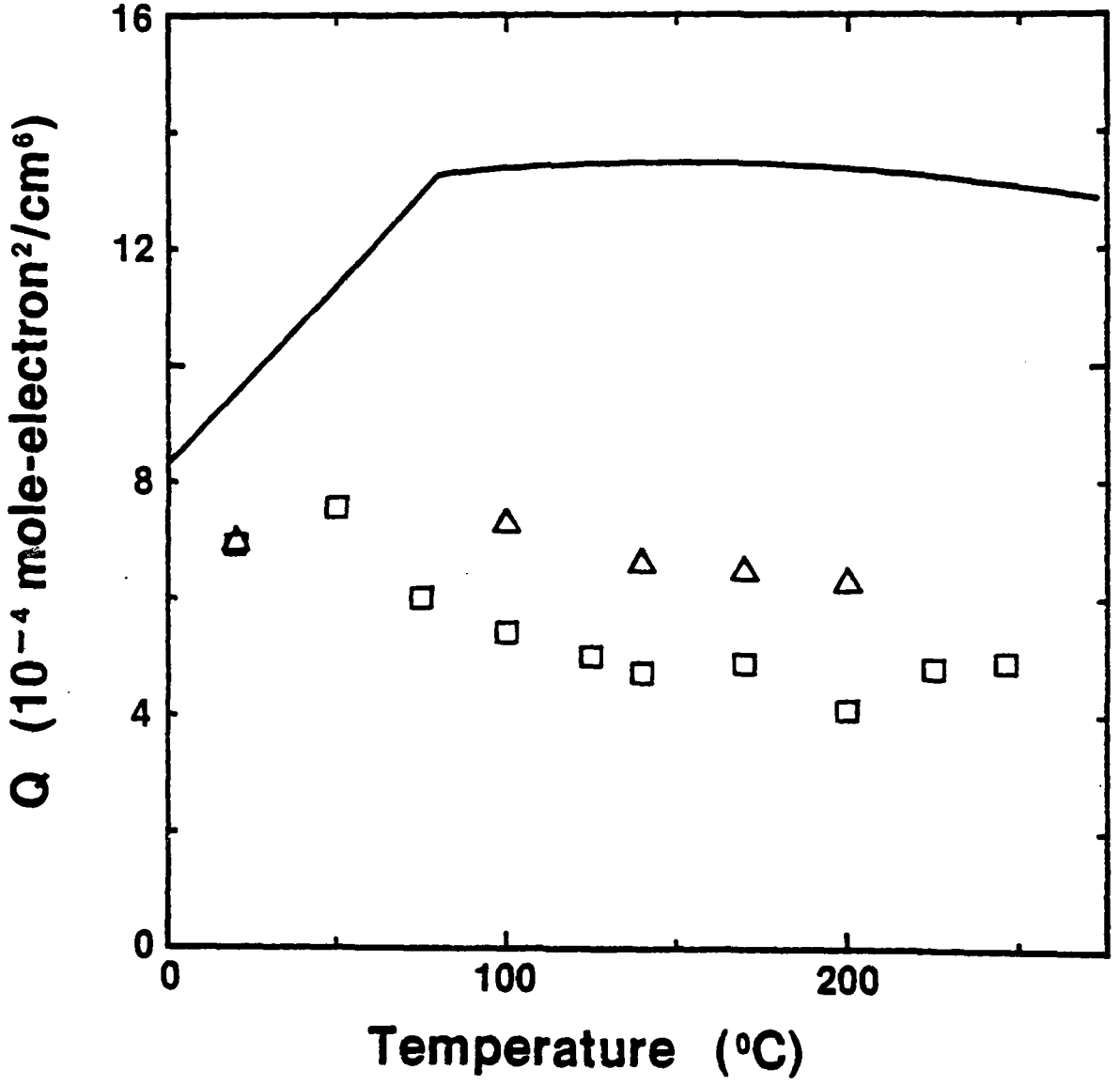

Fig. 10

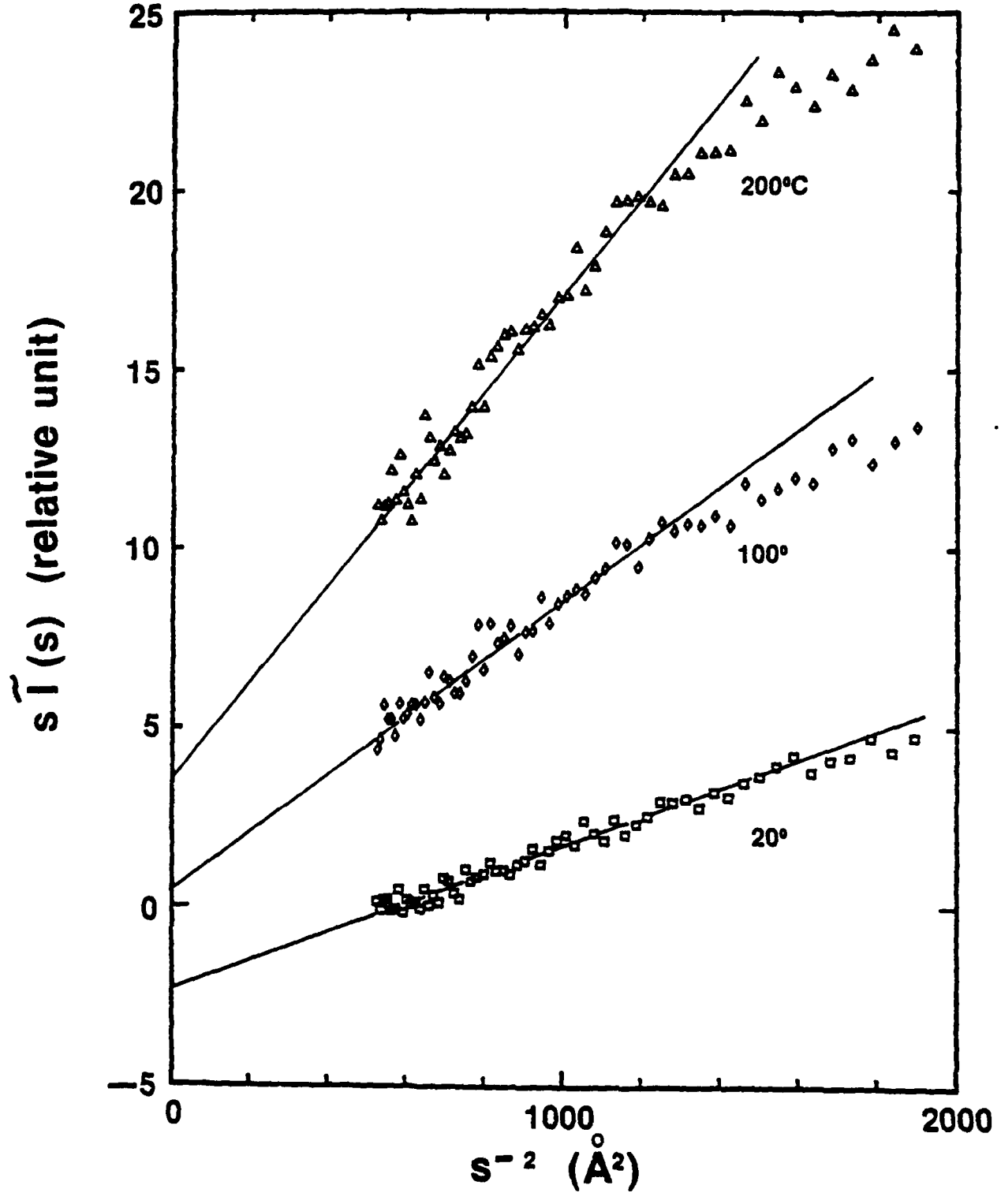

Fig. 11

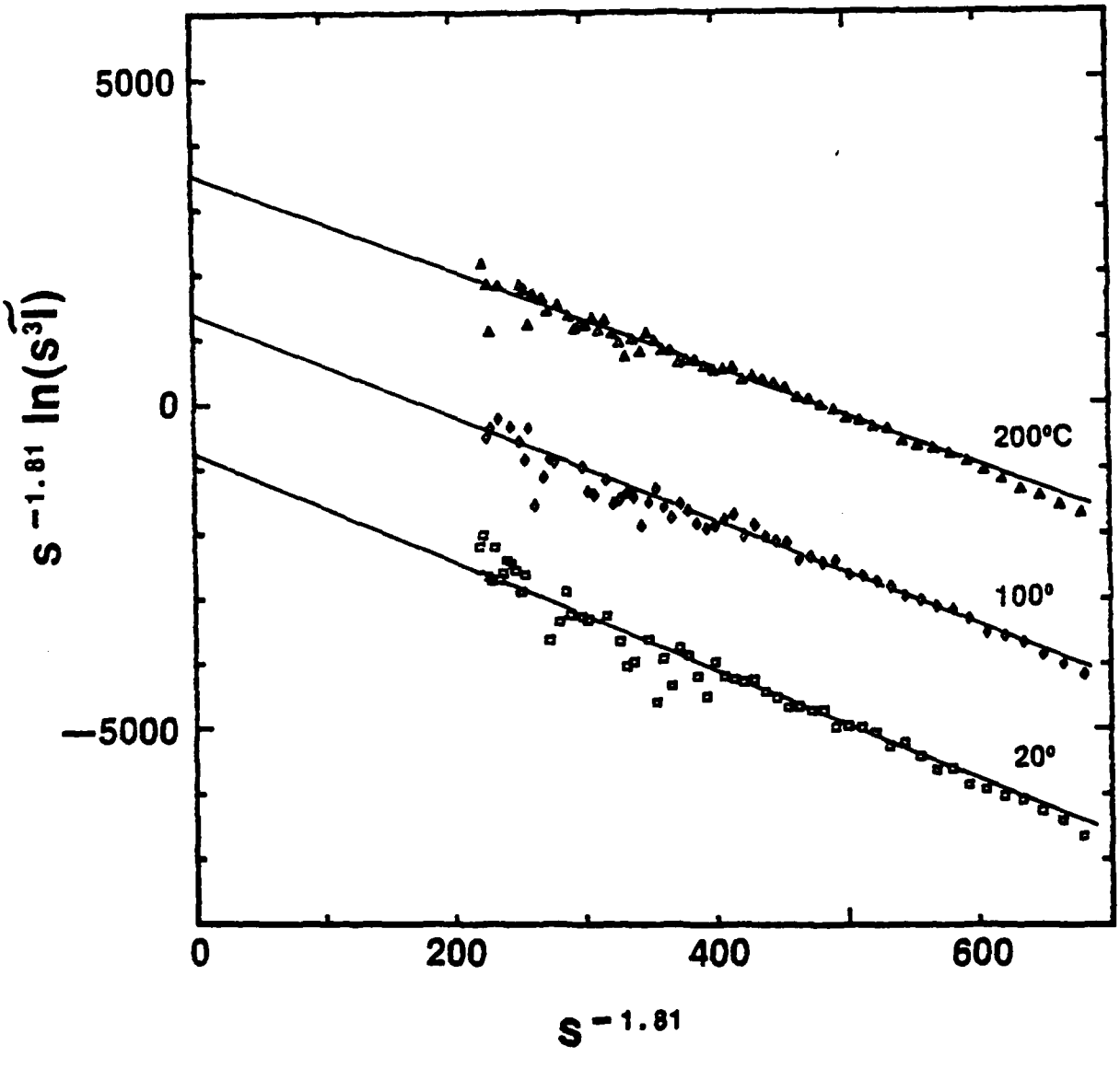

Fig. 12

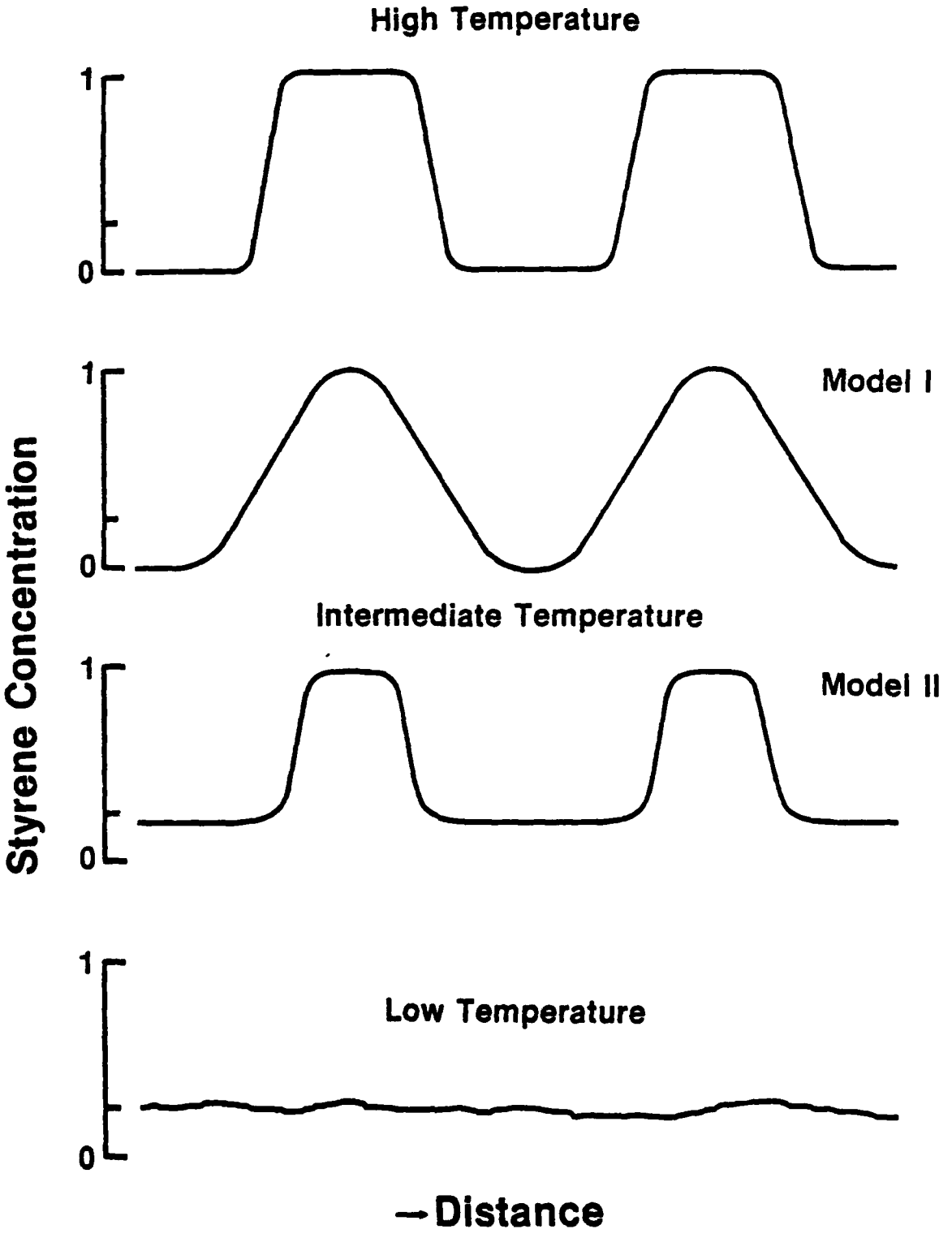
High Temperature
1
0
1
0
Model I
Intermediate Temperature
1
0
Model II
Styrene Concentration
1
0
Low Temperature
Distance

Fig. 13

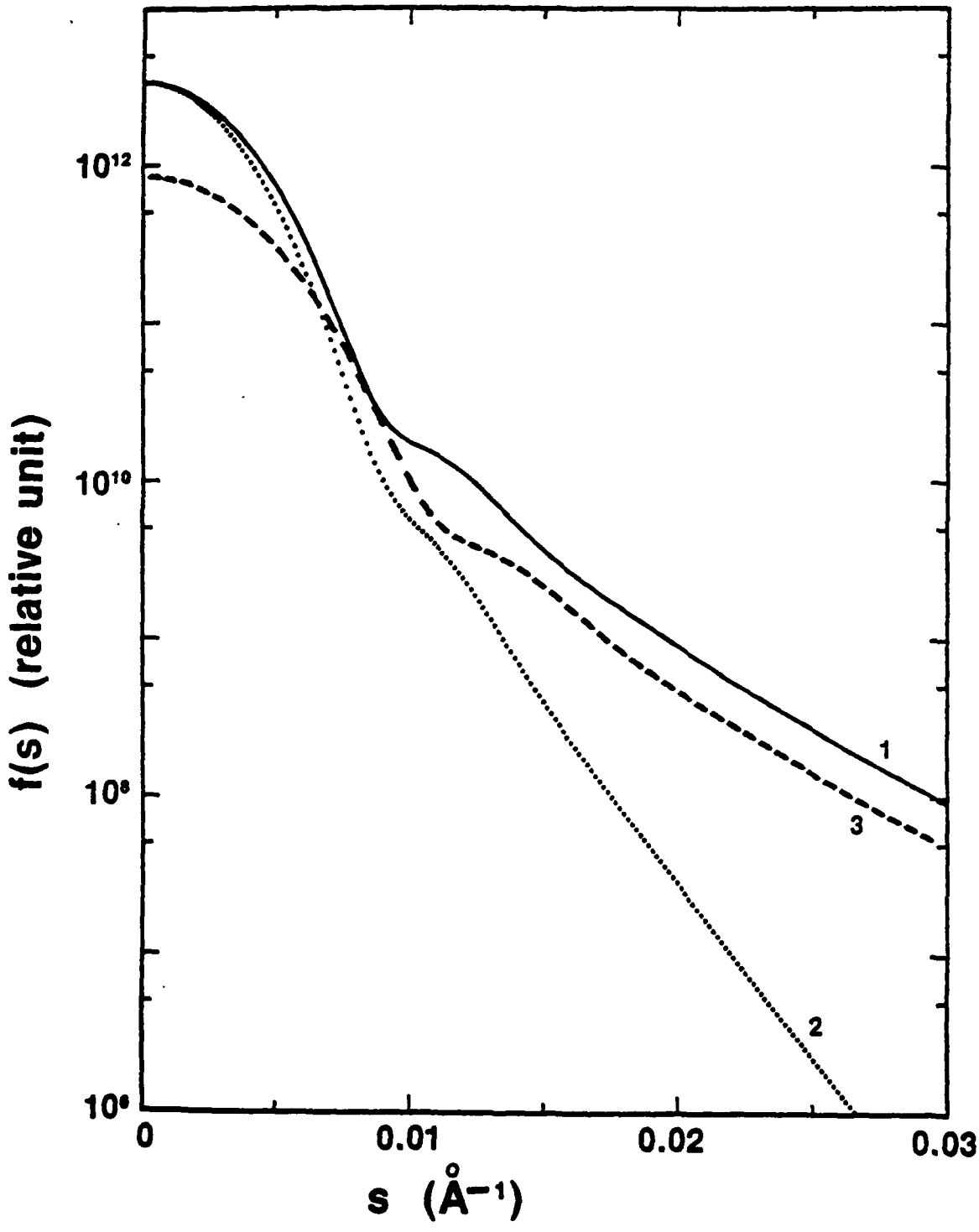

Fig. 14

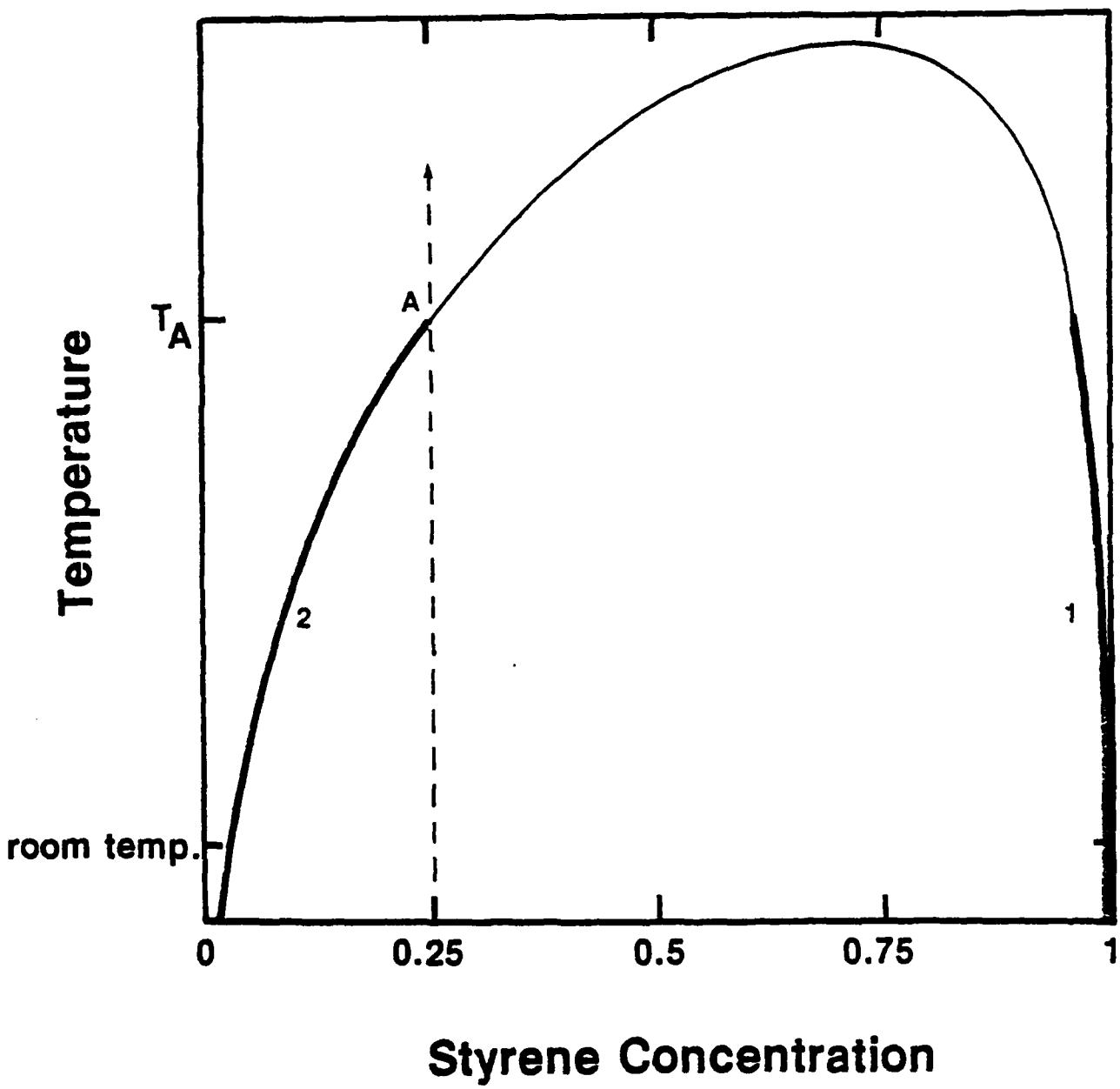
Temperature
T_A
A
room temp.
2
1
0
0.25
0.5
0.75
1
Styrene Concentration

Fig. 15

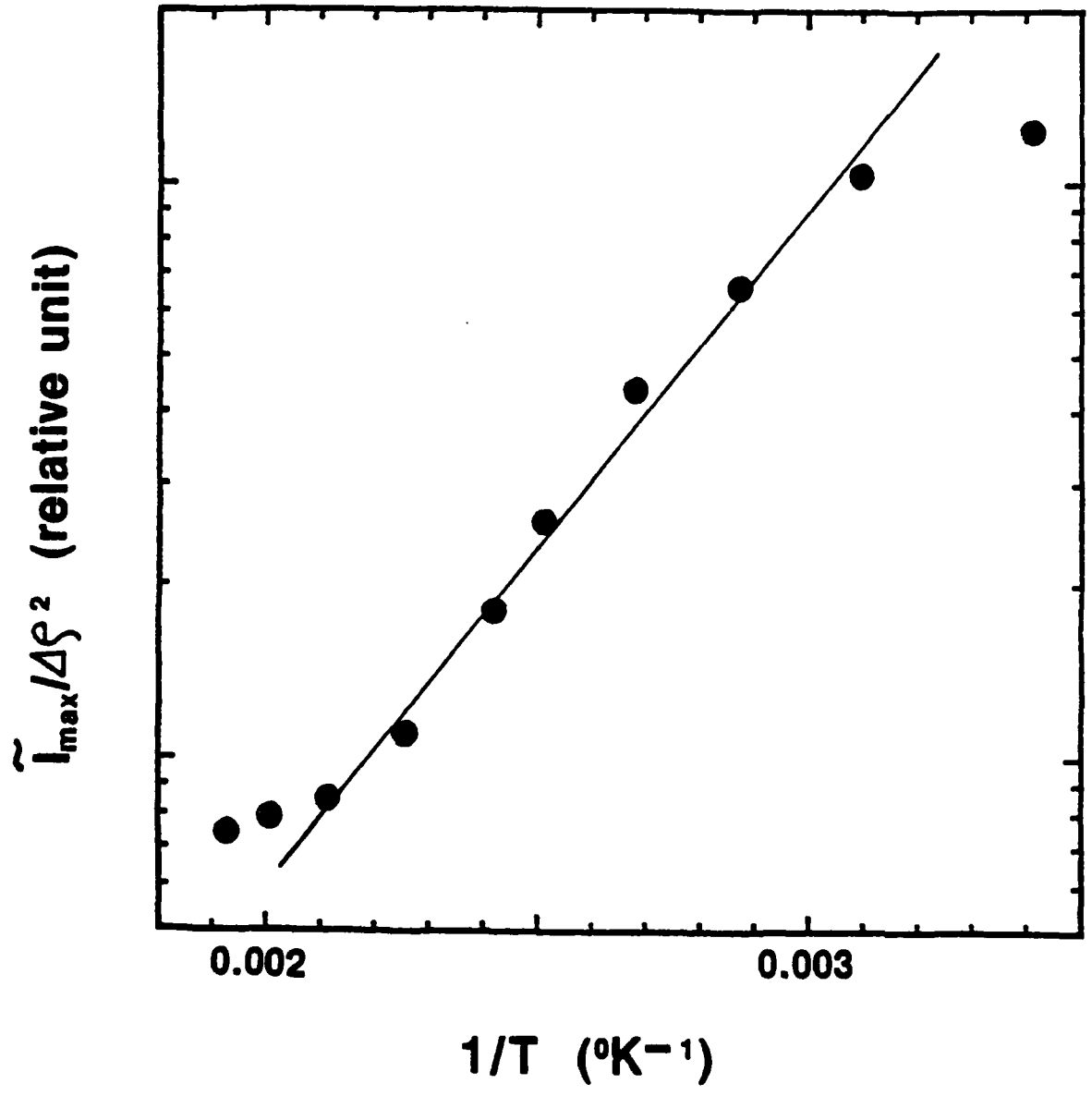

SP472-3/A1

472:GAN:716:ddc
78u472-608

TECHNICAL REPORT DISTRIBUTION LIST, GEN

	No. Copies
Office of Naval Research Attn: Code 472 800 North Quincy Street Arlington, Virginia 22217	2
ONR Branch Office Attn: Dr. George Sandoz 536 S. Clark Street Chicago, Illinois 60605	1
ONR Area Office Attn: Scientific Dept. 715 Broadway New York, New York 10003	1
ONR Western Regional Office 1030 East Green Street Pasadena, California 91106	1
ONR Eastern/Central Regional Office Attn: Dr. L. H. Peebles Building 114, Section D 666 Summer Street Boston, Massachusetts 02210	1
Director, Naval Research Laboratory Attn: Code 6100 Washington, D.C. 20390	1
The Assistant Secretary of the Navy (RE&S) Department of the Navy Room 4E736, Pentagon Washington, D.C. 20350	1
Commander, Naval Air Systems Command Attn: Code 310C (H. Rosenwasser) Department of the Navy Washington, D.C. 20360	1
Defense Technical Information Center Building 5, Cameron Station Alexandria, Virginia 22314	12
Dr. Fred Saalfeld Chemistry Division, Code 6100 Naval Research Laboratory Washington, D.C. 20375	1
U.S. Army Research Office Attn: CRD-AA-IP P.O. Box 1211 Research Triangle Park, N.C. 27709	1
Naval Ocean Systems Center Attn: Mr. Joe McCartney San Diego, California 92152	1
Naval Weapons Center Attn: Dr. A. B. Amster, Chemistry Division China Lake, California 93555	1
Naval Civil Engineering Laboratory Attn: Dr. R. W. Drisko Port Hueneme, California 93401	1
Department of Physics & Chemistry Naval Postgraduate School Monterey, California 93940	1
Dr. A. L. Slafkosky Scientific Advisor Commandant of the Marine Corps (Code RD-1) Washington, D.C. 20380	1
Office of Naval Research Attn: Dr. Richard S. Miller 800 N. Quincy Street Arlington, Virginia 22217	1
Naval Ship Research and Development Center Attn: Dr. G. Bosmajian, Applied Chemistry Division Annapolis, Maryland 21401	1
Naval Ocean Systems Center Attn: Dr. S. Yamamoto, Marine Sciences Division San Diego, California 91232	1
Mr. John Boyle Materials Branch Naval Ship Engineering Center Philadelphia, Pennsylvania 19112	1

TECHNICAL REPORT DISTRIBUTION LIST, GEN

	No. Copies
Dr. Rudolph J. Marcus Office of Naval Research Scientific Liaison Group American Embassy APO San Francisco 96503	1
Mr. James Kelley DTNSRDC Code 2803 Annapolis, Maryland 21402	1

TECHNICAL REPORT DISTRIBUTION LIST, 356A

	No. Copies
Dr. Stephen H. Carr Department of Materials Science Northwestern University Evanston, Illinois 60201	1
Dr. M. Broadhurst Bulk Properties Section National Bureau of Standards U.S. Department of Commerce Washington, D.C. 20234	2
Professor G. Whitesides Department of Chemistry Massachusetts Institute of Technology Cambridge, Massachusetts 02139	1
Professor J. Wang Department of Chemistry University of Utah Salt Lake City, Utah 84112	1
Dr. V. Stannett Department of Chemical Engineering North Carolina State University Raleigh, North Carolina 27607	1
Dr. D. R. Uhlmann Department of Metallurgy and Material Science Massachusetts Institute of Technology Cambridge, Massachusetts 02139	1
Naval Surface Weapons Center Attn: Dr. J. M. Augl, Dr. B. Hartman White Oak Silver Spring, Maryland 20910	1
Dr. G. Goodman Globe Union Incorporated 5757 North Green Bay Avenue Milwaukee, Wisconsin 53201	1
Professor Hatsuo Ishida Department of Macromolecular Science Case-Western Reserve University Cleveland, Ohio 44106	1
Picatinny Arsenal Attn: A. M. Anzalone, Building 3401 SMUPA-FR-M-D Dover, New Jersey 07801	1
Dr. J. K. Gillham Department of Chemistry Princeton University Princeton, New Jersey 08540	1
Douglas Aircraft Co. Attn: Technical Library C1 290/36-84 AUTO-Sutton 3855 Lakewood Boulevard Long Beach, California 90846	1
Dr. E. Baer Department of Macromolecular Science Case Western Reserve University Cleveland, Ohio 44106	1
Dr. K. D. Pae Department of Mechanics and Materials Science Rutgers University New Brunswick, New Jersey 08903	1
NASA-Lewis Research Center Attn: Dr. T. T. Serofini, MS-49-1 21000 Brookpark Road Cleveland, Ohio 44135	1
Dr. Charles H. Sherman Code TD 121 Naval Underwater Systems Center New London, Connecticut	1
Dr. William Risen Department of Chemistry Brown University Providence, Rhode Island 02192	1
Dr. Alan Gent Department of Physics University of Akron Akron, Ohio 44304	1

TECHNICAL REPORT DISTRIBUTION LIST, 356A

	No. Copies
Mr. Robert W. Jones Advanced Projects Manager Hughes Aircraft Company Mail Station D 132 Culver City, California 90230	1
Dr. C. Giori IIT Research Institute 10 West 35 Street Chicago, Illinois 60616	1
Dr. M. Litt Department of Macromolecular Science Case Western Reserve University Cleveland, Ohio 44106	1
Dr. R. S. Roe Department of Materials Science and Metallurgical Engineering University of Cincinnati Cincinnati, Ohio 45221	1
Dr. Robert E. Cohen Chemical Engineering Department Massachusetts Institute of Technology Cambridge, Massachusetts 02139	1
Dr. T. P. Conlon, Jr., Code 3622 Sandia Laboratories Sandia Corporation Albuquerque, New Mexico	1
Dr. Martin Kaufmann, Head Materials Research Branch, Code 4542 Naval Weapons Center China Lake, California 93555	1
Professor S. Senturia Department of Electrical Engineering Massachusetts Institute of Technology Cambridge, Massachusetts 02139	1
Dr. T. J. Reinhart, Jr., Chief Composite and Fibrous Materials Branch Nonmetallic Materials Division Department of the Air Force Air Force Materials Laboratory (AFSC) Wright-Patterson AFB, Ohio 45433	1
Dr. J. Lando Department of Macromolecular Science Case Western Reserve University Cleveland, Ohio 44106	1
Dr. J. White Chemical and Metallurgical Engineering University of Tennessee Knoxville, Tennessee 37916	1
Dr. J. A. Manson Materials Research Center Lehigh University Bethlehem, Pennsylvania 18015	1
Dr. R. F. Helmreich Contract RD&E Dow Chemical Co. Midland, Michigan 48640	1
Dr. R. S. Porter Department of Polymer Science and Engineering University of Massachusetts Amherst, Massachusetts 01002	1
Professor Garth Wilkes Department of Chemical Engineering Virginia Polytechnic Institute and State University Blacksburg, Virginia 24061	1
Dr. Kurt Baum Fluorochem Inc. 6233 North Irwindale Avenue Azuza, California 91702	1
Professor C. S. Paik Sung Department of Materials Sciences and Engineering Room 8-109 Massachusetts Institute of Technology Cambridge, Massachusetts 02139	1


END
DATE
FILMED
DTIC

AD-A094 531 CINCINNATI UNIV OH DEPT OF MATERIALS SCIENCE AND MET--ETC F/G 7/4
SMALL-ANGLE X-RAY DIFFRACTION STUDY OF THERMAL TRANSITION IN ST--ETC(U)
JAN 81 R ROE, M FISHKIS, J C CHANG N00014-77-C-0376
UNCLASSIFIED TR-5 NL

2 OF 2
AD A 094531

END
DATE FILMED
4-81
DTIC

SUPPLEMENTARY

INFORMATION

CORRECTION

OFFICE OF NAVAL RESEARCH

Contract N00014-77-C-0376

Task No. NR 356-655

TECHNICAL REPORT NO. 5

Small-Angle X-Ray Diffraction Study of Thermal Transition in Styrene-Butadiene Block Copolymers

by

Ryong-Joon Roe, M. Fishkis

and J. C. Chang

Department of Materials Science and

Metallurgical Engineering

University of Cincinnati

Cincinnati, OH 45221

Prepared for Publication

in Macromolecules

January 15, 1981

Please substitute the attached Fig. 12 for the one in the original report.

Fig. 12

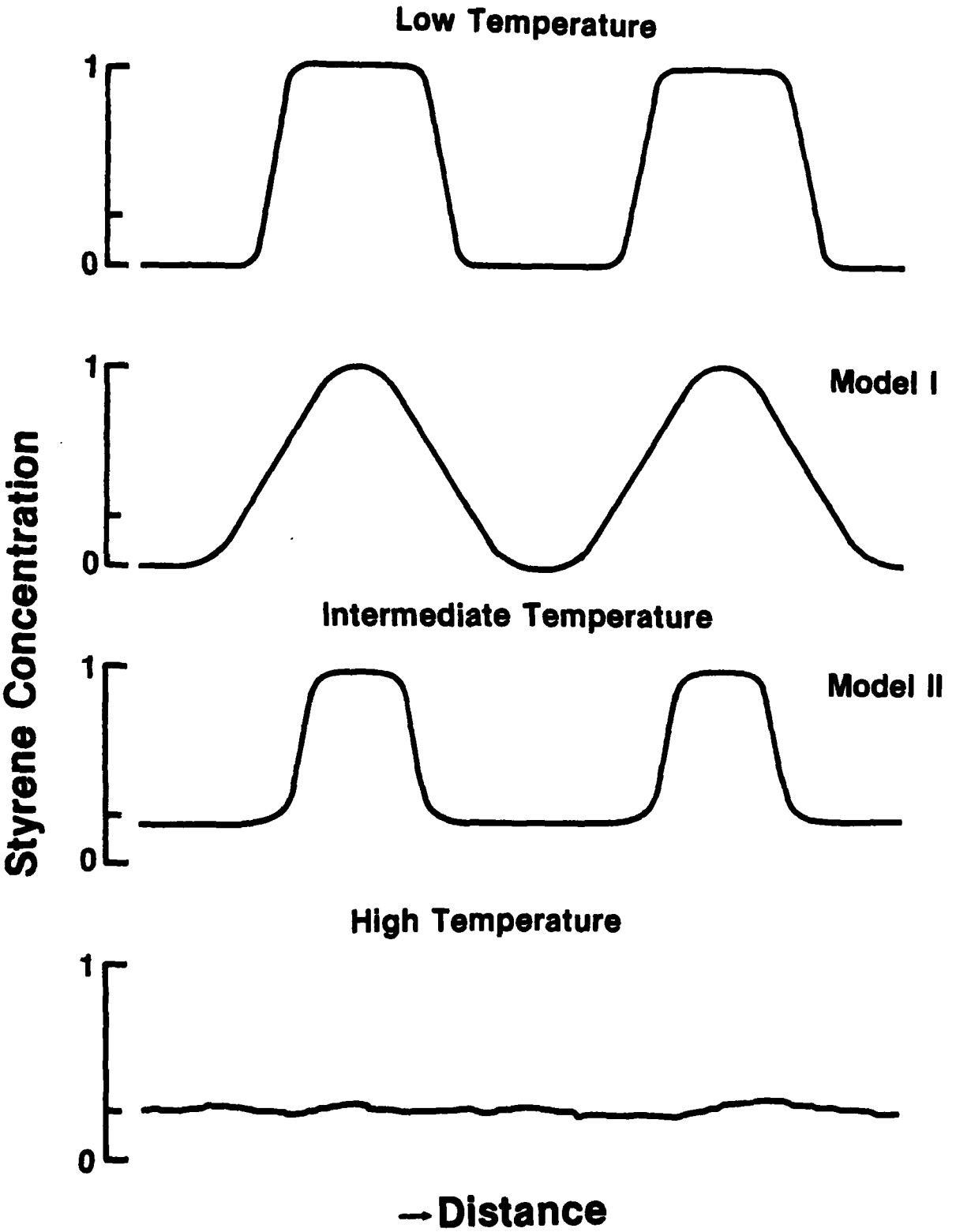
Low Temperature
1
0
Model I
Intermediate Temperature
Model II
High Temperature
Styrene Concentration
Distance

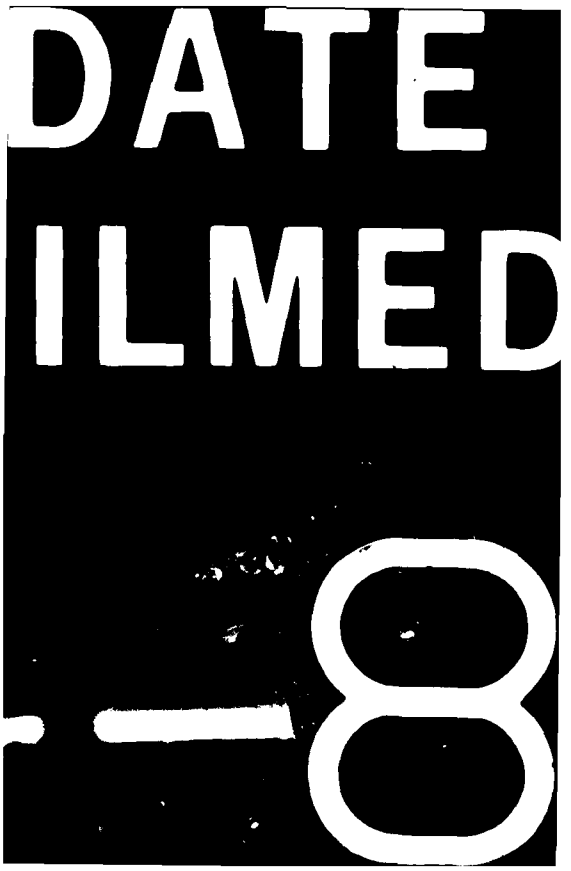
DATE
ILMED
8